

Bayesian Inference from Rank Data

Øystein Sørensen¹, Valeria Vitelli¹, Arnaldo Frigessi^{1,2}, and Elja Arjas^{1,3}

¹Oslo Center for Biostatistics and Epidemiology, Department of
Biostatistics, University of Oslo, Norway

²Oslo Center for Biostatistics and Epidemiology, Research Support Services,
Oslo University Hospital, Norway

³Department of Mathematics and Statistics, University of Helsinki, Finland

Author's Footnote

Øystein Sørensen is PhD student, Oslo Center for Biostatistics and Epidemiology, Department of Biostatistics, University of Oslo, P.O.Box 1122 Blindern, NO-0317 Oslo, Norway (e-mail: oystein.sorensen@medisin.uio.no); Valeria Vitelli is Post Doctoral Fellow, Oslo Center for Biostatistics and Epidemiology, Department of Biostatistics, University of Oslo, P.O.Box 1122 Blindern, NO-0317 Oslo, Norway (e-mail: valeria.vitelli@medisin.uio.no); Arnaldo Frigessi is Professor, Oslo Center for Biostatistics and Epidemiology, University of Oslo and Oslo University Hospital, Norway (e-mail: arnaldo.frigessi@medisin.uio.no); and Elja Arjas is Professor Emeritus, Department of Mathematics and Statistics, University of Helsinki, P.O. Box 68 (Gustaf Hällströmin katu 2b), FI-00014 University of Helsinki, Finland, and Visiting Professor, Oslo Center for Biostatistics and Epidemiology, Department of Biostatistics, University of Oslo, P.O.Box 1122 Blindern, NO-0317 Oslo, Norway (e-mail: elja.arjas@helsinki.fi).

Abstract

Modeling and analysis of rank data has received renewed interest in the era of big data, when recruited or volunteer assessors compare and rank objects to facilitate decision making in disparate areas, from politics to entertainment, from education to marketing. The Mallows rank model is among the most successful approaches, but for computational convenience its use has been limited to a particular form based on the Kendall distance. We develop computationally tractable methods for Bayesian inference in Mallows models with any right-invariant metric, allowing greatly extended flexibility. Our method allows inference on the consensus rankings of the considered items, also when based on data provided in the form of partial rankings, such as top- t or pairwise comparisons. If the assumption of an underlying common true ranking for all assessors is unrealistic, we can find by means of suitable clustering more homogeneous subgroups and consider consensus rankings within each. Our method allows making probabilistic predictions on the classification of assessors based on the ranking of some items, and on individual preferences based only on partial information. Finally, we construct a regression framework for ranks which vary over time. The performance of the approach is studied using several experimental and benchmark datasets, and on simulated data.

Key words— Highly Structured Stochastic Systems, Incomplete Rankings, Mallows Model, Pairwise Comparisons, Preference Learning

1 Introduction

Various types of data have ranks as their natural scale. The manufacturing industry recruits panels to rank novel products, and market studies are often based on interviews where competing products are compared or ranked. In the era of big data, analysing preference data (e.g., movie preferences, restaurant rankings, political candidates, ...) receives much attention. In addition, converting continuous data to ranks can lead to more robust inference when absolute scales are not easily comparable, as in the case of genomic data. For example, Afsari et al. (2014) classify phenotypes based on ranked RNA expressions, and the ARACNE algorithm (Margolin et al., 2006) uses ranked mutual information between pairs of genes to reconstruct gene regulatory networks. For the general background on statistical methods for rank data up to the mid 1990's, we refer to the excellent monograph by Marden (1995).

Two of the most used models for preference learning are the Plackett-Luce (Luce, 1959; Plackett, 1975) and Mallows models (Mallows, 1957). Caron and Teh (2012) perform Bayesian inference in a Plackett-Luce model with time-dependent preferences, and further develop the framework in Caron et al. (2014), where a Dirichlet process mixture is used to cluster assessors based on their preferences. Meilă and Chen (2010) use Dirichlet process mixtures to perform clustering in the Mallows model, and Lu and Boutilier (2011) cluster via the EM algorithm, while also allowing for data in the form of pairwise preferences. Jacques and Biernacki (2014) also propose clustering of possibly partial rankings, but in the context of the Insertion Sorting Rank (ISR) model, and they develop an R package called *Rankcluster* for running their method (Jacques et al., 2014). Most work on Mallows models has been limited to one particular form of the model which uses the Kendall distance, for which the normalizing constant can be computed analytically. Except for computational considerations, there is no reason to believe that other metrics, like the footrule or Spearman distance, would be less powerful or useful than Kendall's.

We develop a Bayesian framework for inference in Mallows models with any right-invariant metric. The normalizing constant is computed offline, using an efficient impor-

tance sampling scheme. Full Bayesian inference is based on a Metropolis-Hastings algorithm designed for rank data. Using data augmentation techniques, our methods also allow for incomplete data like top- t rankings, pairwise comparisons, and ranks missing at random. By being fully Bayesian, we produce coherent posterior credibility levels of learned rankings.

In Section 2, we introduce the Bayesian Mallows model for rank data, give an overview of previous work and discuss modeling issues like the choice of distance measure and prior distribution. In Section 3, we show how efficient Bayesian computation can be performed for this model, using a novel leap-and-shift proposal distribution. We develop an importance sampling scheme for computing the normalizing constant. Section 4 presents our potato experiment, which illustrates the use of the Mallows model for data in the form of full rankings. In Section 5 we extend our model to partial rankings. Section 6 considers data in the form of ordered subsets or pairwise comparisons of items. In Section 7 we describe a mixture model to deal with the possible heterogeneity of assessors and to find cluster-specific consensus rankings. Section 8 is dedicated to class and preference prediction, meaning that both class assignment of new assessors and personalized preference learning is carried out. In Section 9 we analyze ranks which vary over time. Each section has a case study, including the potato experiment, mRNA expression data, football teams, the Movielens film rank data, and a sushi dataset. In Section 10 we perform some simulation experiments in order to gain further insight into how the model works when applying different distance measures. Section 11 presents some conclusions and extensions.

2 A Bayesian Mallows Model for Ranks

Assume we have a set of n items, represented by $\mathbf{A} = \{A_1, A_2, \dots, A_n\}$. Each of N assessors is asked to rank them individually with respect to a considered feature. The ordering provided by assessor j is represented by \mathbf{X}_j , whose n components are items in \mathbf{A} . The item with rank 1 appears as the first element, up to the item with rank n appearing as the n th

element. Our observations $\mathbf{X}_1, \dots, \mathbf{X}_N$ are now N permutations of the labels in \mathbf{A} . Let $R_{ij} = \mathbf{X}_j^{-1}(A_i)$, $i = 1, \dots, n$, $j = 1, \dots, N$ denote the rank given to item A_i by assessor j , and let $\mathbf{R}_j = (R_{1j}, R_{2j}, \dots, R_{nj})$, $j = 1, \dots, N$ denote the full set of ranks given to the items by assessor j . Letting \mathcal{P}_n be the set of all permutations of $\{1, \dots, n\}$, we have $\mathbf{R}_j \in \mathcal{P}_n$, $j = 1, \dots, N$. Finally, let $d(\cdot, \cdot) : \mathcal{P}_n \times \mathcal{P}_n \rightarrow [0, \infty)$ be a distance measure on the space of n -dimensional permutations.

Mallows models (Mallows, 1957) are non-uniform joint distributions for \mathbf{R} on \mathcal{P}_n , of the form $P(\mathbf{R}|\alpha, \boldsymbol{\rho}) = Z_n(\alpha, \boldsymbol{\rho})^{-1} \exp\{-(\alpha/n)d(\mathbf{R}, \boldsymbol{\rho})\} 1_{\mathcal{P}_n}(\mathbf{R})$, where $\boldsymbol{\rho} \in \mathcal{P}_n$, α is a positive scale parameter, $Z_n(\alpha, \boldsymbol{\rho})$ is a normalizing constant, and $1_S(\cdot)$ is the indicator function of the set S . We assume that the N observed rankings $\mathbf{R}_1, \dots, \mathbf{R}_N$ are conditionally independent given the latent ranking $\boldsymbol{\rho}$, and that each of them follows the Mallows model with parameters $\boldsymbol{\rho}$ and α . The likelihood takes the form

$$P(\mathbf{R}_1, \dots, \mathbf{R}_N|\alpha, \boldsymbol{\rho}) = Z_n(\alpha, \boldsymbol{\rho})^{-N} \exp\left\{\frac{-\alpha}{n} \sum_{j=1}^N d(\mathbf{R}_j, \boldsymbol{\rho})\right\} \prod_{j=1}^N \{1_{\mathcal{P}_n}(\mathbf{R}_j)\}. \quad (1)$$

2.1 Distance Measures and Normalizing Constants

If the metric $d(\cdot, \cdot)$ is right-invariant, i.e., invariant to an arbitrary relabeling of the items (Diaconis, 1988, p. 112), the normalizing constant is independent of $\boldsymbol{\rho}$, so we can write $Z_n(\alpha, \boldsymbol{\rho}) = Z_n(\alpha) = \sum_{\mathbf{R} \in \mathcal{P}_n} \exp\{-(\alpha/n)d(\mathbf{R}, \mathbf{P})\}$, where $\mathbf{P} \in \mathcal{P}_n$ is arbitrary. Since this is a sum of $n!$ terms, analytic computation is in general intractable when n is larger than about 10. The Kendall distance measures the minimum number of pairwise adjacent transpositions which convert \mathbf{R} into \mathbf{P} , and its normalizing constant simplifies to $Z_n(\alpha) = \prod_{i=1}^n \sum_{j=0}^{i-1} e^{-\alpha j/n}$, which is computationally feasible also when n is large. For this reason, most applications of Mallows models have been restricted to Kendall distance (Lu and Boutilier, 2011; Meilă and Chen, 2010), except for cases in which the number of items is very small (Murphy and Martin, 2003). However, other metrics have been suggested for particular applications. Important right-invariant metrics are the footrule dis-

tance, $d(\mathbf{R}, \mathbf{P}) = \sum_{i=1}^n |R_i - P_i|$, and the Spearman distance $d(\mathbf{R}, \mathbf{P}) = \sum_{i=1}^n (R_i - P_i)^2$. Other examples are the Hamming distance, the Ulam distance and the Cayley distance (Marden, 1995, pp. 23-27). The computation of the normalizing constant in the Mallows model when using these distances is NP-complete, and no exact form is known which avoids the summation over $n!$ terms. Asymptotic approximations have been studied in Mukherjee (2013), and they have proved to be useful at least in the movie data example (see Section 8.2). In all other examples the number of items is not large enough to justify asymptotic approximations, but an importance sampling scheme can be efficiently used to approximate $Z_n(\alpha)$ to an arbitrary precision. Importantly, since the normalizing constant $Z_n(\alpha)$ does not depend on $\boldsymbol{\rho}$, it can be computed offline over a grid for α , given n . We remark that other clever approaches for the computation of the normalizing constant, for instance based on pseudo-marginal representations (Andrieu and Roberts, 2009), are also conceivable.

2.2 Prior Distributions

The Bayesian framework allows incorporation of prior knowledge about the ranks $\boldsymbol{\rho}$ and the parameter α . When no prior knowledge exists about $\boldsymbol{\rho}$, an obvious choice is the uniform distribution over \mathcal{P}_n , $\pi(\boldsymbol{\rho}) = (1/n!)1_{\mathcal{P}_n}(\boldsymbol{\rho})$. Specifying the prior distribution for α , on the other hand, can benefit from some reasoning. In the Mallows model we have terms of the form $\exp\{(-\alpha/n)d(R_{ij}, \rho_i)\}$ contributing multiplicatively to the likelihood. To get some idea of what numerical values of α would seem reasonable a priori, we can consider how likely it could be that the rank R_{ij} given by some assessor j to item A_i deviates from the rank ρ_i by at least $n/2$. Using the footrule distance, this would correspond to $d(R_{ij}, \rho_i) = n/2$. We would then have the likelihood contribution $\exp\{(-\alpha/n)d(R_{ij}, \rho_i)\} = \exp\{-\alpha/2\}$, and can thus specify our prior mean for α such that it corresponds to our prior belief that an assessment could be off the mark by $n/2$. For example, with a mean of $\alpha = 10$, the likelihood contribution would be a little bit less than one percent. We represent this using the exponential distribution $\pi(\alpha) = \lambda \exp(-\lambda\alpha)1_{[0, \infty)}(\alpha)$, with hyperparameter $\lambda = 1/10$. Since the footrule distance d_F

and Kendall distance d_K are related by the inequality $d_K \leq d_F \leq 2d_K$ (Diaconis and Graham, 1977, Th. 2), we use $\lambda = 1/10$ when working with the Kendall distance as well. For the Spearman distance, similar reasoning corresponds to $d(R_{ij}, \rho_j) = n^2/4$, so we set $\lambda = n/20$. We show in Section S2.4 of the supplementary material that in some applications considered in this paper, the results are reasonably insensitive to small changes in the hyperparameter λ .

3 Metropolis-Hastings Algorithm

Given prior distributions $\pi(\boldsymbol{\rho})$ and $\pi(\alpha)$, the posterior distribution for $\boldsymbol{\rho}$ and α is

$$P(\boldsymbol{\rho}, \alpha | \mathbf{R}_1, \dots, \mathbf{R}_N) \propto \frac{\pi(\boldsymbol{\rho}) \pi(\alpha)}{Z_n(\alpha)^N} \exp \left\{ -\frac{\alpha}{n} \sum_{j=1}^N d(\mathbf{R}_j, \boldsymbol{\rho}) \right\}.$$

In order to obtain samples from it, we iterate two steps. Starting at $\alpha \geq 0$, $\boldsymbol{\rho} \in \mathcal{P}_n$, we propose $\boldsymbol{\rho}'$ according to a symmetric leap-and-shift distribution described in Section 3.1, and accept it with probability

$$\min \left\{ 1, \frac{\pi(\boldsymbol{\rho}')}{\pi(\boldsymbol{\rho})} \exp \left[\frac{-\alpha}{n} \sum_{j=1}^N \{d(\mathbf{R}_j, \boldsymbol{\rho}') - d(\mathbf{R}_j, \boldsymbol{\rho})\} \right] \right\}. \quad (2)$$

The leap-and-shift distribution ensures a sufficient acceptance ratio by inducing small permutations of elements of $\boldsymbol{\rho}$, while keeping $\boldsymbol{\rho}' \in \mathcal{P}_n$. Next, we propose α' according to $\mathcal{N}(\alpha, \sigma_\alpha^2)$, and accept it with probability

$$\min \left\{ 1, \frac{Z_n(\alpha')^{-N} \pi(\alpha')}{Z_n(\alpha)^{-N} \pi(\alpha)} \exp \left[\frac{-(\alpha' - \alpha)}{n} \sum_{j=1}^N d(\mathbf{R}_j, \boldsymbol{\rho}) \right] \right\},$$

where σ_α^2 can be tuned to obtain a desired acceptance ratio. Note that negative α 's can be proposed, but they are accepted with zero probability because outside the prior support.

Because $Z_n(\alpha)$ does not depend on $\boldsymbol{\rho}$, it can be computed offline on a grid of α values

and interpolated to yield an estimate over a continuous range. Our importance sampling algorithm for this purpose is fully described in Appendix A. We use a directional pseudo-likelihood to sample ranks $\mathbf{R}^1, \dots, \mathbf{R}^K \in \mathcal{P}_n$ at random, where the probability of drawing each \mathbf{R}^k is close to its weight in the sum, $\exp\{(-\alpha/n)d(\mathbf{R}^k, \mathbf{P})\}$. In supplementary Section S11, we show that very good estimates of $Z_n(\alpha)$ are obtained with $K \ll n!$ samples.

3.1 Leap-and-Shift Proposal Distribution

The leap-and-shift proposal distribution, used in (2) to propose a new ranking $\boldsymbol{\rho}'$, is defined as follows. Fix some $L \in \{1, \dots, \lceil n/2 \rceil\}$ and draw a random index u uniformly in $\{1, \dots, n\}$.

Define

$$\mathcal{S} = \begin{cases} \{\rho_u - L, \dots, \rho_u + L\} \setminus \{\rho_u\}, & \text{if } L + 1 \leq \rho_u \leq n - L \\ \{1, \dots, 2L\} \setminus \{\rho_u\}, & \text{if } \rho_u \leq L \\ \{n - 2L + 1, \dots, n\} \setminus \{\rho_u\}, & \text{if } \rho_u \geq n - L + 1, \end{cases}$$

and draw a random number r uniformly in \mathcal{S} . Let $\boldsymbol{\rho}^* \in \mathbb{R}^n$ have elements $\rho_u^* = r$ and $\rho_i^* = \rho_i$ for $i \in \{1, \dots, n\} \setminus \{u\}$. The probability mass function for this *leap step* is

$$\begin{aligned} P_L(\boldsymbol{\rho}^* | \boldsymbol{\rho}) &= \sum_{u=1}^n P_L(\boldsymbol{\rho}^* | U = u, \boldsymbol{\rho}) P(U = u) \\ &= \frac{1}{2nL} \sum_{u=1}^n \left\{ 1_{\{L+1, \dots, n-L\}}(\rho_u) \times 1_{\{\rho_u-L, \dots, \rho_u+L\} \setminus \{\rho_u\}}(\rho_u^*) + 1_{\{1, \dots, L\}}(\rho_u) \right. \\ &\quad \left. \times 1_{\{1, \dots, 2L\} \setminus \{\rho_u\}}(\rho_u^*) + 1_{\{n-L+1, \dots, n\}}(\rho_u) \times 1_{\{n-2L+1, \dots, n\} \setminus \{\rho_u\}}(\rho_u^*) \right\} \times 1_{\{\boldsymbol{\rho}_{-u}\}}(\boldsymbol{\rho}_{-u}^*), \end{aligned}$$

where $\boldsymbol{\rho}_{-u} = (\rho_i \forall i \neq u)$.

By construction, $\boldsymbol{\rho}^* \notin \mathcal{P}_n$, since there exist two indices $i \neq j$ such that $\rho_i^* = \rho_j^*$, and we

need a shift to account for the leap. Define $\Delta = \rho_u^* - \rho_u$ and let $\boldsymbol{\rho}'$ have elements

$$\rho'_i = \begin{cases} \rho_i - 1 & \text{if } \rho_u < \rho_i \leq \rho_u^* \text{ and } \Delta > 0 \\ \rho_i + 1 & \text{if } \rho_u < \rho_i \leq \rho_u^* \text{ and } \Delta < 0 \\ \rho_i & \text{else ,} \end{cases}$$

for $i = 1, \dots, n$. The proposal $\boldsymbol{\rho}' \in \mathcal{P}_n$ is a local perturbation of $\boldsymbol{\rho}$, separated by an Ulam distance of 1 (Marden, 1995, pp. 26-27). The parameter L can be used to tune the acceptance ratio.

4 The Potato Experiment

To illustrate the method, we first consider an experiment where the true value of $\boldsymbol{\rho}$ is known. We bought a bag of potatoes, with a total weight of approximately 1.5 kilograms. The $n = 20$ potatoes were picked out from the bag one at a time at random, and marked by letter codes A, B,...,T. We then spread the potatoes on a table, and asked 12 assessors to rank them according to their weight twice: first by visual inspection, and next he/she was allowed to feel the weight of the potatoes by holding them. The assessors acted independently. Supplementary Figure S1 shows photos from the experiment. We labeled the potatoes A_1, A_2, \dots, A_{20} , and afterwards we weighed each potato, thus deriving the true $\boldsymbol{\rho}$. Based on Section 2.2, we chose the exponential prior with rate $\lambda = 1/10$ when using the footrule and Kendall distance, and $\lambda = n/20$ when using the Spearman distance.

The heat plots in Figure 1 show the posterior probabilities, for all potatoes, for being ranked as the k th heaviest, plotted against their true ranks (latent ranks are along the vertical axis, and true ranks along the horizontal axis). The trace is the posterior expectation of the number of correctly ranked potatoes, $\sum_{i=1}^n 1_{\{\hat{\rho}_i = \rho_i\}} P(\hat{\rho}_i = \rho_i | \text{data})$. In the visual inspection experiment, the Spearman distance had the largest trace, while the Kendall distance had the smallest. In the weighing experiment, the footrule distance performed slightly better than the

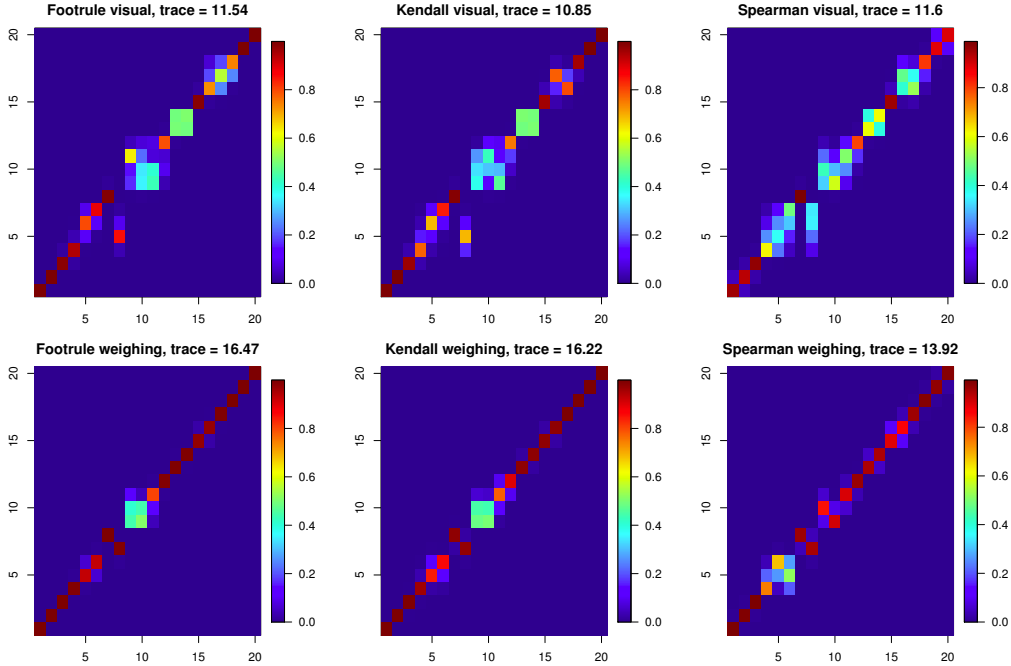


Figure 1: Heat plots of the latent ranks (vertical axis) versus the true rank (horizontal axis) for the potato experiment. The trace represents the posterior expectation of the number of correctly ranked potatoes.

Kendall distance, and both were much better than the Spearman distance. The middle range potatoes were assessed less accurately than those at the extremes, especially in the visual inspection experiment. Supplementary Figures S3 and S4 show posterior histograms for the latent ranks for selected potatoes. The different distance measures performed varyingly in the different situations, but overall the Mallows model with the footrule distance seemed to be the best in order to maximize the expected number of correctly ranked potatoes.

5 Partial Ranking

A situation frequently arising in applications is that only a subset of the items have been ranked. Ranks can be missing at random, or the assessors may only have ranked, say, the top-5 items. These types of situations can be handled fairly easily in our Bayesian framework, by applying data augmentation techniques.

Assume that each assessor j has ranked the items in $\mathcal{A}_j \subseteq \{A_1, A_2, \dots, A_n\}$. Let $R_{ij} =$

$\mathbf{X}_j^{-1}(A_i)$ if $A_i \in \mathcal{A}_j$, and $R_{ij} = \star$ otherwise, $i = 1, \dots, n$, $j = 1, \dots, N$. Our goal is to sample from the posterior distribution

$$P(\alpha, \boldsymbol{\rho} | \mathbf{R}_1, \dots, \mathbf{R}_N) = \sum_{\tilde{\mathbf{R}}_1 \in \mathcal{S}_1} \cdots \sum_{\tilde{\mathbf{R}}_N \in \mathcal{S}_N} P(\alpha, \boldsymbol{\rho} | \tilde{\mathbf{R}}_1, \dots, \tilde{\mathbf{R}}_N) P(\tilde{\mathbf{R}}_1, \dots, \tilde{\mathbf{R}}_N | \mathbf{R}_1, \dots, \mathbf{R}_N).$$

\mathcal{S}_j is the set of allowable 'fill-ins' of the missing ranks in \mathbf{R}_j , $\mathcal{S}_j = \{\tilde{\mathbf{R}}_j \in \mathcal{P}_n : \tilde{R}_{ij} = \mathbf{X}_j^{-1}(A_i) \text{ if } A_i \in \mathcal{A}_j\}$, $j = 1, \dots, n$, so $\tilde{\mathbf{R}}_1, \dots, \tilde{\mathbf{R}}_N$ are augmented rank vectors consistent with the partial observations. $P(\alpha, \boldsymbol{\rho} | \tilde{\mathbf{R}}_1, \dots, \tilde{\mathbf{R}}_N)$ is the posterior joint distribution for α and $\boldsymbol{\rho}$ given the augmented data, and we can sample from it as in Section 3. Fixing the observed ranks $\mathbf{R}_1, \dots, \mathbf{R}_N$ in the full likelihood (1), we see that

$$P(\tilde{\mathbf{R}}_1, \dots, \tilde{\mathbf{R}}_N | \alpha, \boldsymbol{\rho}, \mathbf{R}_1, \dots, \mathbf{R}_N) = \prod_{j=1}^N \frac{1_{\mathcal{S}_j}(\tilde{\mathbf{R}}_j)}{Z_n(\alpha)} \exp\left\{\frac{-\alpha}{n} d(\tilde{\mathbf{R}}_j, \boldsymbol{\rho})\right\}. \quad (3)$$

We can thus alternate between sampling the augmented ranks given the current values of α and $\boldsymbol{\rho}$ from (3), and sampling α and $\boldsymbol{\rho}$ given the current values of the augmented ranks. To propose new values of the unobserved ranks for assessor j , we use a uniform distribution on \mathcal{S}_j .

5.1 Top-5 Estimation in the Potato Experiment

In many applications, the main interest lies in estimating the top- t items, for some number $t < n$. When collecting data, it is important to decide how many top ranks each assessor should identify. Collecting complete ranks is more demanding than asking for only the top items, so this is important in planning of experiments. We thus provide a small illustration of how the top-5 results depend on how many potatoes were ranked. We investigate this in the case of top-10 and top-5 datasets for our potato experiment, by ignoring ranks above 10 or 5, respectively. We focus on the weighing experiment here. See Section S2.3 of the supplementary material for similar results in the visual inspection experiment. As before, we

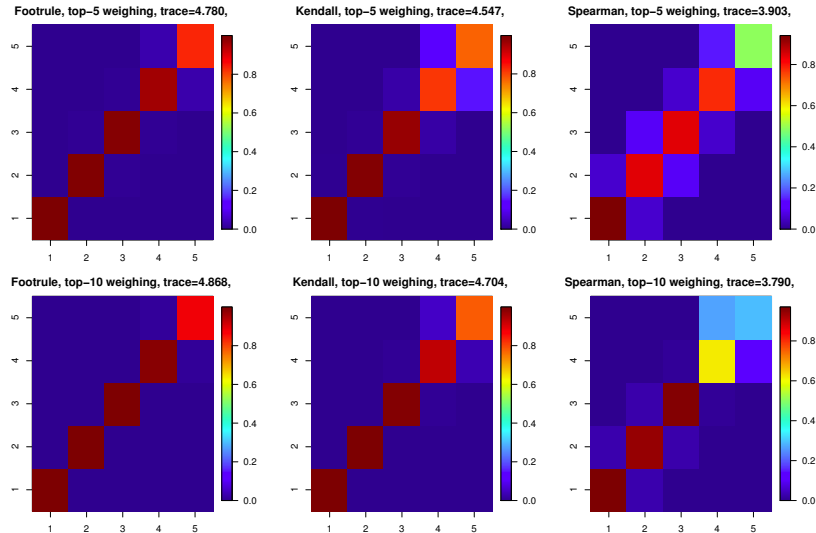


Figure 2: Heat plots of the experiment in Section 5.1: Estimation of the five heaviest potatoes when using only the five heaviest potatoes (top), and when using only the ten heaviest potatoes (bottom).

used an exponential prior with $\lambda = 1/10$ for the footrule and Kendall distance, and $\lambda = n/20$ for the Spearman distance. 12 out of 20 potatoes had been ranked among the top-10 by at least one assessor, but the remaining 8 potatoes were also included in the analysis, as the posterior distribution for their ranks depends on the observed ranks, and similarly for the top-5 experiment. Figure 2 shows heat plots of the estimated five heaviest potatoes, corresponding to the lower left corners in Figure 1. Again the footrule distance provided the best estimates.

5.2 Meta-Analysis of Differential Gene Expression

Studies of differential gene expression between two conditions produce a list of genes, ranked according to their level of differential expression as measured by, e.g., p -value. There is often little overlap between gene lists found by independent studies comparing the same conditions, and it is interesting to find a consensus list over all available studies. Each study $i \in \{1, \dots, N\}$ is an assessor, providing a top- k_i list of differentially expressed genes, and the genes are ranked items. This problem has been studied by DeConde et al. (2006); Deng et al.

Rank	Gene	$P(\rho \leq \text{Rank})$	$P(\rho \leq 10)$
1	HPN	0.05	0.35
2	AMACR	0.06	0.27
3	GDF15	0.07	0.23
4	NME1	0.09	0.23
5	FASN	0.10	0.20
6	EEF2	0.12	0.19
7	UAP1	0.13	0.18
8	KRT18	0.14	0.17
9	OACT2	0.14	0.15
10	NME2	0.14	0.14

Table 1: Finding a consensus of genes across studies: The table shows the top-10 latent ranks based on top-25 lists from five different studies of prostate cancer, comprising a total of 89 genes. The ranking was performed by first finding the gene with highest probability of having $\rho_i = 1$, then, among the remaining genes, the genes with highest probability of having $\rho_i \in \{1, 2\}$, and so on. This cumulative probability is represented by $P(\rho \leq \text{Rank})$. The probability of being among the top-10 is also shown for each gene.

(2014); Lin and Ding (2009), who all used five studies comparing prostate cancer patients with healthy controls (Dhanasekaran et al., 2001; Luo et al., 2001; Singh et al., 2002; True et al., 2006; Welsh et al., 2001). The top-25 lists from each study contained 89 genes in total.

Table 1 shows the result of analyzing the five gene lists with the Mallows footrule model. Like DeConde et al. (2006); Deng et al. (2014); Lin and Ding (2009), our method ranks HPN and AMACR first and second, but otherwise there is little agreement. The low level of agreement between the studies is also illustrated by the posterior distribution for α , with a mean around 0.5. Following Section 2.2, this means that the likelihood contribution of a ranking R_i deviating from ρ_i by $n/2$, is about 78%. Notice also the low posterior probability for each gene to be among the top-10. The original studies measured between 4653 and 7567 genes (DeConde et al., 2006), and these should have been included in our analysis as unranked items, with the effect of making the posterior probabilities in Table 1 smaller. We conclude that these five studies of prostate cancer jointly have led to quite inconclusive evidence about differentially expressed genes.

Other related uses of top- t rankings in genomics are aggregation of gene lists across platforms or across different statistical methods used for the same data (Boulesteix and Slawski, 2009; Kolde et al., 2012).

6 Ordered Subsets and Pairwise Comparisons

In many situations, the data take the form of comparisons between items, rather than a complete ranking, for example when the assessors perform multiple pairwise comparisons. For the Mallows model with the Kendall distance, Lu and Boutilier (2011) have studied the case of pairwise comparisons. We modify our fully Bayesian data augmentation scheme to handle these situations, for any right-invariant distance.

As a simple example of paired comparisons, assume assessor j stated the preferences $\mathcal{B}_j = \{A_1 \prec A_2, A_2 \prec A_5, A_4 \prec A_5\}$. Here $A_r \prec A_s$ means that A_s is preferred to A_r , so that A_s has a lower rank than A_r . Let \mathcal{A}_j be the set of items constrained by assessor j , in this case $\mathcal{A}_j = \{A_1, A_2, A_4, A_5\}$. Differently from Section 5, the constrained items are not necessarily fixed to a given rank. Hence, in the MCMC algorithm, we need to propose augmented ranks which obey the partial ordering constraints given by each assessor, to avoid a large number of rejections. We assume that the pairwise orderings in \mathcal{B}_j are mutually compatible, and denote by $\text{tc}(\mathcal{B}_j)$ the transitive closure of \mathcal{B}_j , containing all pairwise orderings of the elements in \mathcal{A}_j induced by \mathcal{B}_j . In the example, $\text{tc}(\mathcal{B}_j) = \mathcal{B}_j \cup \{A_1 \prec A_5\}$. For the case of ordered subsets of items, the transitive closure is simply the single set of pairwise preferences compatible with the ordering, e.g., $\{A_1 \prec A_2 \prec A_5\}$ yields $\text{tc}(\mathcal{B}_j) = \{A_1 \prec A_2, A_2 \prec A_5, A_1 \prec A_5\}$. The R packages `sets` (Meyer and Hornik, 2009) and `relations` (Meyer and Hornik, 2014) were used to compute transitive closures.

The leap-and-shift algorithm requires an adjustment in order to propose augmented ranks which are consistent with the partial ordering constraints. Suppose that from the last step of the MCMC algorithm, we have a full rank vector $\tilde{\mathbf{R}}_j$ for assessor j , which is consistent with $\text{tc}(\mathcal{B}_j)$. Draw a random number u uniformly in $\{1, \dots, n\}$. If $A_u \in \mathcal{A}_j$, let $l_j = \max\{\tilde{R}_{kj} : A_k \in \mathcal{A}_j, k \neq u, (A_k \succ A_u) \in \text{tc}(\mathcal{B}_j)\}$, with the convention that $l_j = 0$ if the set is empty, and $r_j = \min\{\tilde{R}_{kj} : A_k \in \mathcal{A}_j, k \neq u, (A_k \prec A_u) \in \text{tc}(\mathcal{B}_j)\}$, with the convention that $r_j = n + 1$ if the set is empty. Now complete the leap step by drawing a new proposal \tilde{R}'_{uj} uniformly from the set $\{l_j + 1, \dots, r_j - 1\}$. Otherwise, if $A_u \notin \mathcal{A}_j$, we complete the leap step by drawing

\tilde{R}'_{uj} uniformly in $\{1, \dots, n\}$. The shift step remains unchanged.

6.1 A Premier League Season

The English football Premier League consists of 20 teams, which all play two games against each other. To illustrate the use of paired comparisons, we let the Mallows model with footrule distance give an alternative ranking of the teams, by considering each matchday as an assessor. Each game not ending in a draw is a pairwise preference. Excluding draws in this way, we considerably simplified the modeling of game outcomes. A predictive model for betting would take into account a large number of other factors (draws, home games, etc.), which we have not included at this point. To summarize the joint posterior distribution for the ranks of all teams, we first identified the team with highest marginal posterior probability for having rank 1, then the team with the highest marginal posterior probability for having rank 1 or 2, and so on, see Table 2. The numbers in parentheses show the 90 % highest posterior density intervals (HPDI) for the ranks of each team, representing the posterior uncertainty in the ranking based on the actual game results. Table 2 agrees very well with the official league table of that season, especially in the top and bottom of the table. The HPDIs are very wide, because there is considerable variability in the outcomes of individual games, and because the data are fairly sparse, as each pair of teams meet only twice per season. Other sports have more games in the final rounds. The posterior CDFs for the rankings of all twenty teams (supplementary Figure S9) reveal perfect stochastic orderings between most of the teams, with Manchester United stochastically dominating all others, and West Ham being stochastically dominated by all others. Supplementary Table S5 shows an indicator matrix for all the stochastic orderings.

	Team	CP	90 % HPDI				
1	Man. United	0.31	(1,5)	11	Bolton	0.42	(6,19)
2	Chelsea	0.31	(1,8)	12	Newcastle	0.50	(7,20)
3	Man. City	0.45	(1,8)	13	Sunderland	0.57	(7,20)
4	Arsenal	0.58	(1,8)	14	Stoke City	0.62	(8,20)
5	Tottenham	0.61	(1,9)	15	Blackburn	0.61	(9,20)
6	Everton	0.48	(1,13)	16	Wigan	0.67	(8,20)
7	Liverpool	0.51	(1,13)	17	Birmingham	0.65	(10,20)
8	Fulham	0.45	(2,16)	18	Blackpool	0.75	(10,20)
9	Aston Villa	0.36	(4,18)	19	Wolverhampton	0.87	(11,20)
10	West Bromwich	0.39	(5,19)	20	West Ham	1.00	(13,20)

Table 2: Premier League teams arranged by their cumulative probability (CP) in the Mallows model, with 90 % highest posterior density intervals.

7 Clustering Assessors Based on Full Rankings

So far we have assumed that there exists a unique consensus ranking shared by all assessors. In many cases the assumption of homogeneity of assessors with respect to an underlying common true ranking is unrealistic (e.g., consumer preferences, movie rankings), and the possibility of dividing them into more homogeneous subsets, each sharing preferences on the items, makes the model closer to reality. We handle this using a mixture of Mallows models. In the frequentist framework, mixtures of Mallows models have been used to analyze heterogeneous rank data (Busse et al., 2007; Lu and Boutilier, 2011; Murphy and Martin, 2003), while Bayesian approaches have been limited to the Plackett-Luce (Caron et al., 2014) and generalized Mallows models (Meilă and Chen, 2010).

Let $z_1, \dots, z_N \in \{1, \dots, C\}$ assign each assessor to one of C clusters. The assessments within each cluster $c \in \{1, \dots, C\}$, are described by a Mallows model with parameters α_c and ρ_c . Assuming conditional independence across the clusters, the augmented data formulation of the likelihood for the observed rankings $\mathbf{R}_1, \dots, \mathbf{R}_N$ is given by

$$P\left(\mathbf{R}_1, \dots, \mathbf{R}_N \mid \{\rho_c, \alpha_c\}_{c=1}^C, z_1, \dots, z_N\right) = \prod_{j=1}^N \frac{1_{\mathcal{P}_n}(\mathbf{R}_j)}{Z_n(\alpha_{z_j})} \exp\left\{\frac{-\alpha_{z_j}}{n} d(\mathbf{R}_j, \rho_{z_j})\right\}.$$

For the scale parameters, we assume the prior $\pi(\alpha_1, \dots, \alpha_C) \propto \lambda^C \exp(-\lambda \sum_{c=1}^C \alpha_c)$ $1_{\{\alpha_1 < \dots < \alpha_C\}}(\alpha_1, \dots, \alpha_C)$. The constraint $\alpha_1 < \dots < \alpha_C$ ensures cluster identifiability (Jasra et al., 2005). We further assume that the cluster labels are a priori distributed according to $P(z_1, \dots, z_N \mid \tau_1, \dots, \tau_C) = \prod_{j=1}^N \tau_{z_j}$, where τ_c is the probability that an assessor belongs

	$c = 1$	$c = 2$	$c = 3$	$c = 4$	$c = 5$	$c = 6$
τ_c (%)	19 (17,21)	9.0 (7.3,10)	24 (22,26)	5.4 (4.6,6.1)	4.2 (4.0,5.0)	38 (36,41)
α_c	1.6 (1.5,1.6)	1.8 (1.7,2.0)	2.9 (2.8,3.1)	2.9 (2.8,3.2)	3.1 (3.0,3.3)	3.9 (3.8,4.2)
	sea urchin fatty tuna sea eel salmon roe shrimp tuna squid tuna roll egg cucumber roll	fatty tuna tuna sea urchin salmon roe tuna roll squid shrimp sea eel egg cucumber roll	fatty tuna tuna sea eel shrimp tuna roll squid egg cucumber roll salmon roe sea urchin	shrimp egg squid sea eel cucumber roll salmon roe tuna roll fatty tuna tuna sea urchin	salmon roe fatty tuna tuna tuna roll egg shrimp squid cucumber roll sea eel sea urchin	fatty tuna sea urchin salmon roe tuna shrimp sea eel tuna roll squid egg cucumber roll

Table 3: Sushi items arranged according to the MAP estimates of the cluster centers, and the corresponding MAP estimates for τ (in %) and α (with 95% HPDIs).

to the c -th subpopulation; $\tau_c \geq 0$, $c = 1, \dots, C$ and $\sum_{c=1}^C \tau_c = 1$. Finally τ_1, \dots, τ_C are assigned the standard symmetric Dirichlet prior $\pi(\tau_1, \dots, \tau_C) = \Gamma(\psi C) \Gamma(\psi)^{-C} \prod_{c=1}^C \tau_c^{\psi-1}$. We sample the resulting posterior distribution using an MCMC algorithm detailed in the supplementary material. The number of clusters C is usually not known, and here we select C by inspecting the posterior distribution of the within-cluster sum-of-squares of the distances of the observed ranks from the corresponding cluster center.

7.1 Sushi Data

We illustrate clustering based on full rankings using a benchmark dataset of sushi preferences collected across Japan (Kamishima, 2003), see also Lu and Boutilier (2011). $N = 5000$ people were interviewed, each giving a complete ranking of $n = 10$ sushi variants. Cultural differences among Japanese regions influence food preferences, so we expect the assessors to be clustered around different preferences. We analyzed the sushi data using mixtures of Mallows models with the footrule or Spearman distance, showing results from the latter in Section S5 of the supplementary material. In the Dirichlet prior for τ , we set $\psi = 2$, thus favoring high-entropy distributions. For each candidate $C \in \{1, \dots, 10\}$, we used a random subset of MCMC samples to compute the posterior footrule distance between ρ_c and the ranking of each assessor assigned to cluster c , for $c = 1, \dots, C$. The posterior sum of squares of such within-cluster distances over all assessors and cluster centers, i.e. $\sum_{c=1}^C \sum_{j:z_j=c} d(\mathbf{R}_j, \rho_c)^2$, was used for choosing an appropriate value for C , see Figure 3 (left). We found an elbow at $C = 6$, which was then used. Table 3 reports the maximum

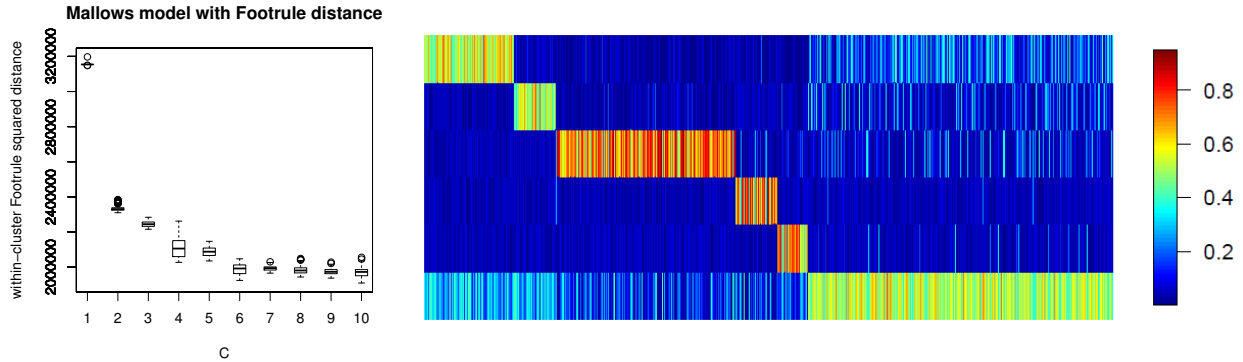


Figure 3: Left: Boxplots of the posterior distributions of the within-cluster sum-of-squares distances of assessors from the corresponding cluster center for different choices of C . Right: Heatplot of posterior probabilities for all 5000 assessors (on the x-axis) of being assigned to each cluster ($c = 1, \dots, 6$ from top to bottom).

a posteriori (MAP) estimates for τ and α , together with their 95% HPDIs, and the sushi items arranged as in the MAP estimate for cluster centers.

We can also investigate the stability of the clustering. Figure 3 (right) shows a heatplot of posterior probabilities, for all 5000 assessors (shown on the x-axis), for being assigned to each of the $C = 6$ clusters identified by the MAP estimate of Table 3 (clusters $c = 1, \dots, C$ from top to bottom in Figure 3). As shown by the heatplot, most of these individual probabilities were concentrated on some particular preferred value of c among the six possibilities, indicating a reasonably stable behavior in the cluster assignments. The three clusters with the highest posterior uncertainty in assignment of assessors were $c = 1, 2, 6$. We refer to Section S5 in the supplementary material for some additional observations on this dataset.

8 Class and Preference Prediction

In this Section we consider two important situations, where rank data are used to make individual level predictions. The first one is the rank version of a classical classification problem: we train a Bayesian classifier by using known feature and class membership information on individuals (here assessors) belonging to a training set, and then we use the classifier to

predict the unknown class membership of individuals (new assessors) belonging to a test set. The second problem is a version of feature prediction, where the features are preferences expressed by individual customers, now serving in the role of assessors, on a considered set of items. Of most interest to us here is the situation in which customers have provided only partial information on their preferences. The task is then to synthesize this information, in order to predict the preferences of other individuals about whom information is possibly even less complete. Both these situations can be treated within our Bayesian Mallows model.

8.1 Classification of Breast Cancer Patients into Disease Subtypes

Assume that for a subset $\mathcal{T} \subset \{1, \dots, N\}$ of $N_T < N$ assessors, the true class is known. Fixing the cluster indicators $\{z_j\}_{j \in \mathcal{T}}$, and using the multinomial prior for $\{z_j\}_{j \notin \mathcal{T}}$, the posterior distribution for $\{z_j\}_{j \notin \mathcal{T}}$ can be used as a discriminant function for the class memberships of the remaining $N - N_T$ assessors. The classification rule may be, e.g., to assign $j \notin \mathcal{T}$ to the class corresponding to the MAP estimate for z_j . In this setting, the clusters are identifiable, and no constraints on α_c are needed. For simplicity, however, a single dispersion parameter α , shared by all classes, was used in the examples of this section.

Rank-based classification in genomics has seen a growing interest recently (Afsari et al., 2014; Tan et al., 2005), because it eases comparison across different technologies and studies. We illustrate our method on a dataset with mRNA expression values of $n = 98$ genes involved in the KEGG *estrogen signaling pathway*, with $N = 102$ breast cancer patients (Naume et al., 2007). The patients were either estrogen receptor negative (ER-, 35 patients) or positive (ER+, 67 patients), and our aim was to predict the ER status of future breast cancer patients (which is relevant information for their treatment) based on the ranked expressions of these 98 genes. The MAP estimate for z_j , $j \notin \mathcal{T}$, was used as the classification rule, and the classification error of the procedure was estimated using leave-one-out cross-validation.

The proportion of misclassified patients was 17.6% (13 false ER-, 5 false ER+). The posterior probability for assignment to ER+ for the 5 misclassified ER- patients was in the

range $[0.72, 0.85]$, much lower than for all other correctly assigned ER+ patients, for whom it was larger than 0.975. For 9 out of the 13 misclassified ER+ patients, the posterior probability for assignment to ER- was in the range $[0.5, 0.68]$, while for the correctly assigned ER- patients it was larger than 0.992. Assessing the posterior uncertainty of each patient’s class assignment is thus very useful in evaluating the risk of misclassification, possibly suggesting the need for further clinical tests before treatment. In Section S6 of the supplementary material we further explore the misclassification rates discussed above in the light of the associated ROC curve.

8.2 Prediction of Individual Preferences: The Movielens Data

Another important problem concerns individual prediction of preferences. In machine learning, the subfield named *preference learning* has the scope of learning a predictive preference model from observed preference information (Furnkranz and Hullermeier, 2011). In many situations, a training set is constructed with a set of assessors who have made extensive paired comparisons or even full rankings. Based on these, we want to predict the preferences for new assessors, who have made just a small number of paired comparisons. This case is very relevant in many applications, where a curated training set is available, and the preferences of many new assessors have to be predicted (Francis et al., 2010), as in online video streaming, see for example the Netflix competition (netflixprize.com). We can use the Bayesian mixture of Mallows models for prediction of preferences, with the necessary extensions to deal with partial rankings or pairwise comparisons. If assessor j has compared only a subset of items, $P(\tilde{\mathbf{R}}_j|\text{all data})$ represents posterior predictive probabilities about his/her full rankings. These posterior probabilities are directly obtained from our MCMC algorithms, see equation (3). For example, if assessor j did not compare A_1 to A_2 , we might be interested in $P(A_1 \prec_j A_2|\text{all data})$, which is readily obtained from $P(\tilde{\mathbf{R}}_j|\text{all data})$. Here, ' \prec_j ' denotes a preference of assessor j .

The Movielens dataset (www.grouplens.org/datasets/) contains movie ratings from

6040 users. In this illustrative example, we focused on the $n = 200$ most rated movies, and on the $N = 5891$ users who rated at least 3 of these movies, and converted ratings from a 1-5 scale to pairwise preferences discarding ties, as in Lu and Boutilier (2011). We divided the N users into 14 classes, depending on age and gender (see supplementary Section S7). In many applications classes are also estimated, but here we used predefined classes for simplicity. We applied for these data the Mallows models with the footrule distance. With $n = 200$, the importance sampling scheme for $Z_n(\alpha)$ was not efficient, and we implemented the asymptotic approximation described in Mukherjee (2013).

Each user had considered only a subset of the movies (30.2 on average). We tested the method by discarding, from each assessor j , one of the rated movies at random, while using all the other rated movies and class membership to compute $P(\tilde{\mathbf{R}}_j | \text{all data})$. To evaluate our method, for each assessor j we randomly selected one of the pairwise preferences involving the discarded movie, and computed the posterior probability for correctly predicting the discarded preference. The median, across all assessors, of the posterior probabilities of correctly predicting the discarded preference was 0.81. Moreover, 87.3 % of these probabilities were higher than 0.5. Some further insight and analyses on this dataset can be found in Section S7 of the supplementary material.

9 Modeling of Time-Dependent Ranks

There are many situations in which rankings vary over time, as in political surveys (Regenwetter et al., 1999) or book bestsellers (Caron and Teh, 2012). Our approach can be extended to this setting. Assume we have observed ranks at discrete timepoints indexed by $t = 0, 1, \dots, T$. Let $\boldsymbol{\rho}^{(t)}$ and $\alpha^{(t)}$ denote the parameters at time t , and let $\mathbf{R}_j^{(t)}$, $j = 1, \dots, N_t$, denote the ranks observed at time t , where N_t is the number of assessors at time t . We

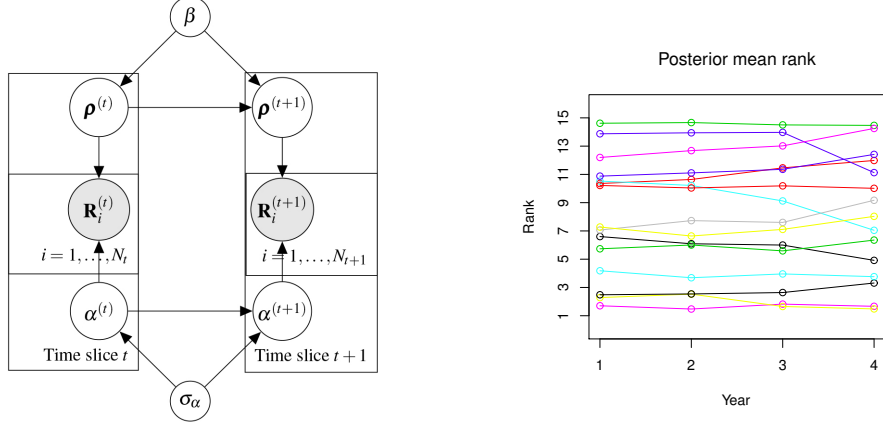


Figure 4: Left: The time dependent rank model represented by a dynamic Bayesian network. Right: The development of the mean ranks of each student over the four school years analyzed in the example of Section 9.1.

model the transition between latent ranks with the Mallows model,

$$P\{\boldsymbol{\rho}^{(t)}|\boldsymbol{\rho}^{(t-1)}, \beta\} = Z_n(\beta)^{-1} \exp\left[\frac{-\beta}{n}d\{\boldsymbol{\rho}^{(t)}, \boldsymbol{\rho}^{(t-1)}\}\right] 1_{\mathcal{P}_n}\{\boldsymbol{\rho}^{(t)}\}, \quad t = 1, \dots, T, \quad (4)$$

where β describes how strongly the ranks at time t depend on the ranks at time $t - 1$. We assume that the observed ranks at time t are conditionally independent of the observed ranks at all other times, given $\boldsymbol{\rho}^{(t)}$ and $\alpha^{(t)}$, yielding the likelihood contribution $P\{\mathbf{R}_1^{(t)}, \dots, \mathbf{R}_{N_t}^{(t)}|\alpha^{(t)}, \boldsymbol{\rho}^{(t)}\} = Z_n\{\alpha^{(t)}\}^{-1} \exp[-\{\alpha^{(t)}/n\}d\{\mathbf{R}^{(t)}, \boldsymbol{\rho}^{(t)}\}]$, for $t = 0, \dots, T$, and the complete data likelihood

$$P\{\text{data}|\alpha^{(0:T)}, \boldsymbol{\rho}^{(0:T)}\} = \prod_{t=0}^T \left(Z_n\{\alpha^{(t)}\}^{-N_t} \prod_{j=1}^{N_t} \exp\left[\frac{-\alpha^{(t)}}{n}d\{\mathbf{R}_j^{(t)}, \boldsymbol{\rho}^{(t)}\}\right] \right),$$

where $(t_1 : t_2)$ denotes all time points from t_1 up to and including t_2 . Finally, we model the transition process of α with the normal distribution and a positivity constraint, $P\{\alpha^{(t)}|\alpha^{(t-1)}, \sigma_\alpha\} \sim \mathcal{N}\{\alpha^{(t-1)}, \sigma_\alpha^2\} \times 1_{\mathbb{R}^+}\{\alpha^{(t)}\}$, $t = 1, \dots, T$. For $\rho^{(0)}$ we use the uniform prior, and for $\alpha^{(0)}$ and β , an exponential prior with the same rate, for simplicity. For σ_α^2 we use an inverse gamma distribution, $P(\sigma_\alpha^2) = IG(a, b)$, with shape $a = 1$ and scale $b = 1$. The conditional independence properties assumed in this model are depicted in Figure 4 (left).

9.1 Student Data

In this illustration we consider 15 students enrolled in a high school program in Italy. Top-ranked students will be most attractive for further studies or the job market. We obtained results of all tests in mathematics over their first four years in the school: 5, 4, 8, and 8 tests, respectively. The tests scores were numbers between 0 (worst) and 10 (best). 15 of the 375 values were missing, and we imputed them using the Gibbs sampler implemented in the R package `mice` (van Buuren and Groothuis-Oudshoorn, 2011). Each test was considered an assessor, and the scores were converted to ranks. There were many ties in the data, which were handled by drawing random complete rankings consistent with the data at regular intervals in the MCMC algorithm. We used the Mallows model with the Spearman distance, and an exponential prior with rate $\lambda = n/20$.

Figure 4 (right) shows how the mean ranks of the 15 students developed over the four-year period. We see that the performance of most students was smooth over the first two years, but from the third to the fourth year there were some whose rank within the class changed considerably. Further results on this examples can be found in Section S8 in the supplementary material. In situations involving a larger number of items it might be useful, by a further elaboration of the methods presented in Section 7, to form clusters of items with similar profiles in their behavior over time.

10 Simulation Experiments

The results of the potato experiment, where the true ranks were known to us, give some hints about the comparative performances of the Mallows models with footrule, Kendall, and Spearman distances. In order to do a more systematic analysis, we also performed simulation experiments. Define the true ranking $\boldsymbol{\rho} = (1, \dots, n)$. The observations \mathbf{R}_j , $j = 1, \dots, n$, were generated by running $\boldsymbol{\rho}$ through N_{leap} independent sequences of moves of the leap-and-shift algorithm. We used the values $L = 1$ and $L = 5$ for the leap parameter.

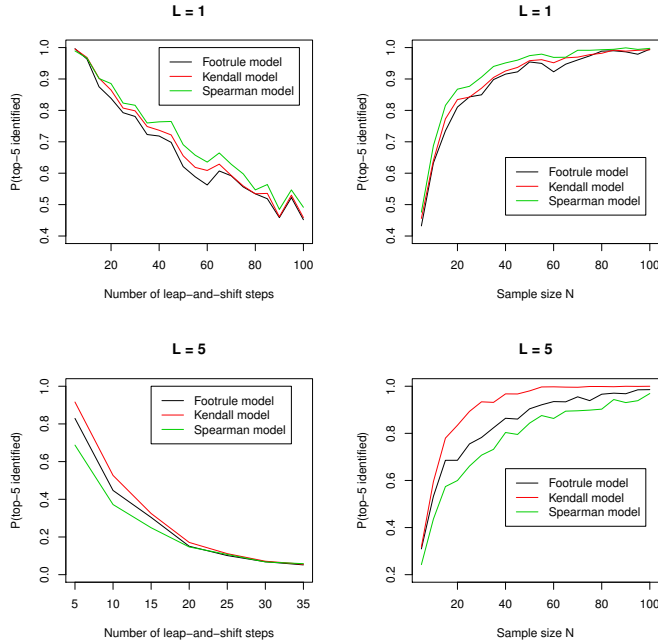


Figure 5: Probability of identifying the top-5 items as the number of leap-and-shift moves used to generate each observation increases (left), and as N increases (right).

$L = 1$ implies that in each move of the algorithm, only neighboring items can be shuffled. $L = 5$, on the other hand, means that items which originally are further away from each other also can be interchanged. We first investigated how the noise level in the data influences the results by varying the number of leap-and-shift moves applied in the data generation, while fixing $N = 10$ and $n = 20$. In the $L = 1$ case the number of moves N_{leap} was gradually increased from 5 to 100, and in the $L = 5$ case from 5 to 35, in steps of size 5. Next, we investigated how the number of assessors influences the results, keeping the number of leap-and-shift moves fixed at 50 in the $L = 1$ case and at 10 in the $L = 5$ case, while increasing N from 5 to 100 in steps of size 5. We computed the posterior probability for correctly identifying the top-5 items in each of 200 independent Monte Carlo simulations.

The left plots in Figure 5 show the results for varying numbers of leap-and-shift moves. With $L = 1$, the Spearman distance performed best, followed by the Kendall and footrule distance. In the $L = 5$ case, the Kendall distance showed the best performance. The right plots show how the results varied with the sample size, and not surprisingly, the quality of

the results improved with increasing N . Also, the comparative performances of the different Mallows models were very similar to the plots on the left-hand side. When $L = 1$, the Spearman distance was the best, followed by the Kendall and footrule distances, while when $L = 5$, the Kendall distance was best, followed by the footrule and Spearman distances.

We can interpret the differences between the models used in Figure S17 by comparing the distance measures. The footrule and Kendall distances are additive, in the sense that perturbing two ranks by one unit off their true value has the same likelihood as perturbing one rank by two units. In other words, if a rank has already been perturbed by one unit, it is as likely to be perturbed by yet another unit off as any other, yet unperturbed rank, by one unit from its true position. In the Spearman distance this is no longer the case, because of the square in the exponent. Thus, if occasional bigger displacements come up in the data, as in the $L = 5$ case, the description given by the Spearman distance is likely to be less fitting. In other words, the inferences provided by the Mallows model with Spearman distance are less robust to larger noise than footrule or Kendall. The Spearman model gives lower posterior probability to latent ranks which are in strong disagreement with some of the assessors, even when the latent rank is in perfect agreement with other assessors.

11 Discussion

In this paper, we have developed a fully Bayesian hierarchical framework for the analysis of rank data. An important advantage of the Bayesian approach, is that it offers coherently propagated and directly interpretable ways to quantify posterior uncertainties of estimates of any quantity of interest. Earlier Bayesian treatments of the Mallows rank model are extended in many ways: we develop an importance sampling scheme for $Z_n(\alpha)$ allowing use of other distances than Kendall's, and our MCMC algorithm efficiently samples from the posterior distribution for the unknown parameters. We have developed various extensions of the model, motivated by particular applications.

The Mallows models considered perform very well with a large number of assessors N , as we show in the sushi example of Section 7, and in the Movielens example of Section 8. On the other hand, they may not be computationally feasible when the number of items is extremely large, e.g. $n \geq 10^4$, which is common for search engines and in ranking of players in online games (Volkovs and Zemel, 2014). For the footrule and Spearman distances, there exist asymptotic approximations for $Z_n(\alpha)$ as $n \rightarrow \infty$ (Mukherjee, 2013), which we used in Section 8, but the MCMC algorithm still needs to explore the space \mathcal{P}_n of $n!$ permutations, which becomes prohibitively expensive when n is very large. Maximum likelihood estimation of $\boldsymbol{\rho}$ runs into the same problem when n gets large (Aledo et al., 2013; Ali and Meilă, 2012). Volkovs and Zemel (2014) developed the multinomial preference model (MPM) for cases with very large n , which can be efficiently computed by maximizing a concave log-likelihood function. The MPM thus seems a useful choice when n is very large and real time performance is needed.

All methods presented have been implemented in C++, and run efficiently on a desktop computer. Obtaining a sufficiently large sample from the posterior distribution takes from a few seconds with the full potato data to several minutes in the examples involving massive data augmentation, e.g., the Premier League data.

When modeling time-dependent ranks in Section 9, we assumed that all items were ranked at each time step. In real situations, it can happen that some items which were not available at time t may become available at later times (Caron and Teh, 2012), like a new movie. Other items might disappear from the pool, like products which are no longer available on the market. If one is interested in the latent ranks of all items at all times, also at time points when they were not assessed, the data augmentation approach of Section 5 could be used. In this way, for an item not being assessed at time t , its observed ranks at other time points would contribute to its latent rank at time t through the transition process (4). If, on the other hand, for a given time point one is only interested in the items which were assessed at that time point, (4) would only take into account the intersection of items present at times

t and $t - 1$.

Inconsistent pairwise preferences also appear in applications. One option is to create mutually compatible preferences by reversing the order of the necessary preference pairs, and let the MCMC algorithm randomly switch among these consistent preference sets.

Many of the extensions we propose for solving specific problems (clustering, preference prediction, pairwise comparisons, ...) might well be needed jointly in real applications. Hence, a useful direction of development would be towards combination of methods, for instance clustering based on pairwise preferences, or prediction of rankings in future time instances. Our general framework is flexible enough to handle these developments quite straightforwardly.

Acknowledgement

The authors thank Thomas Fleischer for providing the breast cancer data, Tyler Lu and Craig Boutilier for their help with the Movielens data, and Magne Thoresen for helpful discussions.

A Appendix: Importance Sampling

For rank vectors $\mathbf{R}^1, \dots, \mathbf{R}^K$ sampled from a proposal distribution $q(\mathbf{R})$, the unbiased importance sampling estimate of $Z_n(\alpha)$ is $\hat{Z}_n(\alpha) = K^{-1} \sum_{k=1}^K \exp\{-(\alpha/n)d(\mathbf{R}^k, \boldsymbol{\rho})\}q(\mathbf{R}^k)^{-1}$. We use a pseudo-likelihood approximation of the target (1), given by the factorization $P(\mathbf{R}|\boldsymbol{\rho}) = P(R_1|R_2, \dots, R_n, \boldsymbol{\rho})P(R_2|R_3, \dots, R_n, \boldsymbol{\rho}) \cdots P(R_{n-1}|R_n, \boldsymbol{\rho})P(R_n|\boldsymbol{\rho})$. The conditionals are

$$P(R_n|\boldsymbol{\rho}) = \frac{\exp\{-(\alpha/n)d(R_n, \rho_n)\} \times 1_{[1, \dots, n]}(R_n)}{\sum_{\tilde{\rho}_n \in \{1, \dots, n\}} \exp\{-(\alpha/n)d(\tilde{\rho}_n, \rho_n)\}},$$

$$P(R_{n-1}|R_n, \boldsymbol{\rho}) = \frac{\exp\{-(\alpha/n)d(R_{n-1}, \rho_{n-1})\} \times 1_{\{1, \dots, n\} \setminus \{R_n\}}(R_{n-1})}{\sum_{\tilde{\rho}_{n-1} \in \{1, \dots, n\} \setminus \{R_n\}} \exp\{-(\alpha/n)d(\tilde{\rho}_{n-1}, \rho_{n-1})\}},$$

$$\begin{aligned} & \vdots \\ P(R_2|R_3, \dots, R_n, \boldsymbol{\rho}) &= \frac{\exp\{-(\alpha/n)d(R_2, \rho_2)\} \times 1_{[\{1, \dots, n\} \setminus \{R_3, \dots, R_n\}]}(R_2)}{\sum_{\tilde{\rho}_2 \in \{1, \dots, n\} \setminus \{R_3, \dots, R_n\}} \exp\{-(\alpha/n)d(\tilde{\rho}_2, \rho_2)\}}, \\ P(R_1|R_2, \dots, R_n, \boldsymbol{\rho}) &= 1_{[\{1, \dots, n\} \setminus \{R_2, \dots, R_n\}]}(R_1). \end{aligned}$$

An \mathbf{R}^k sequentially sampled from these conditionals has probability $q(\mathbf{R}^k) = P(R_n^k|\boldsymbol{\rho}) P(R_{n-1}^k|R_n^k, \boldsymbol{\rho}) \cdots P(R_2^k|R_3^k, \dots, R_n^k, \boldsymbol{\rho})$, where we arbitrarily set $\boldsymbol{\rho} = \{1, \dots, n\}$.

References

- Afsari, B., U. B. Neto, and D. Geman (2014). Rank Discriminants for Predicting Phenotypes from RNA Expression. arXiv:1401.1490 [q-bio.GN].
- Aledo, J. A., J. A. Gàmez, and D. Molina (2013). Tackling the rank aggregation problem with evolutionary algorithms. *Applied Mathematics and Computation* 222, 632 – 644.
- Ali, A. and M. Meilă (2012). Experiments with Kemeny ranking: What works when? *Mathematical Social Sciences* 64(1), 28 – 40. Computational Foundations of Social Choice.
- Andrieu, C. and G. O. Roberts (2009). The pseudo-marginal approach for efficient Monte Carlo computations. *The Annals of Statistics* 37(2), 697–725.
- Boulesteix, A.-L. and M. Slawski (2009). Stability and aggregation of ranked gene lists. *Briefings in Bioinformatics* 10(5), 556–568.
- Busse, L. M., P. Orbanz, and J. M. Buhmann (2007). Cluster analysis of heterogeneous rank data. In *Proceedings of the 24th International Conference on Machine Learning, ICML '07*, New York, NY, USA, pp. 113–120. ACM.
- Caron, F. and Y. W. Teh (2012). Bayesian nonparametric models for ranked data. In F. Pereira, C. J. C. Burges, L. Bottou, and K. Q. Weinberger (Eds.), *Advances in Neural Information Processing Systems 25*, pp. 1520–1528. Curran Associates, Inc.

- Caron, F., Y. W. Teh, and T. B. Murphy (2014). Bayesian nonparametric Plackett-Luce models for the analysis of preferences for college degree programmes. *The Annals of Applied Statistics* 8(2), 1145–1181.
- DeConde, R. P., S. Hawley, S. Falcon, N. Clegg, B. Knudsen, and R. Etzioni (2006). Combining results of microarray experiments: A rank aggregation approach. *Statistical Applications in Genetics and Molecular Biology* 5(1), Article 15.
- Deng, K., S. Han, K. J. Li, and J. S. Liu (2014). Bayesian aggregation of order-based rank data. *Journal of the American Statistical Association* 109(507), 1023–1039.
- Dhanasekaran, S. M., T. R. Barrette, D. Ghosh, R. Shah, S. Varambally, K. Kurachi, K. J. Pienta, M. A. Rubin, and A. M. Chinnaiyan (2001). Delineation of prognostic biomarkers in prostate cancer. *Nature* 412, 822–826.
- Diaconis, P. (1988). *Group representations in probability and statistics*, Volume 11 of *Lecture Notes - Monograph Series*. Hayward, CA, USA: Institute of Mathematical Statistics.
- Diaconis, P. and R. L. Graham (1977). Spearman’s footrule as a measure of disarray. *Journal of the Royal Statistical Society. Series B (Methodological)* 39(2), 262–268.
- Francis, B., R. Dittrich, and R. Hatzinger (2010). Modeling heterogeneity in ranked responses by nonparametric maximum likelihood: how do europeans get their scientific knowledge? *The Annals of Applied Statistics* 4(4), 2181–2202.
- Furnkranz, J. and E. Hullermeier (2011). *Preference Learning*. Springer.
- Jacques, J. and C. Biernacki (2014). Model-based clustering for multivariate partial ranking data. *Journal of Statistical Planning and Inference* 149, 201–217.
- Jacques, J., Q. Grimonprez, and C. Biernacki (2014). Rankcluster: an R package for clustering multivariate partial rankings. *preprint submitted to Elsevier*.

- Jasra, A., C. Holmes, and D. Stephens (2005). Markov chain Monte Carlo methods and the label switching problem in Bayesian mixture modeling. *Statistical Science* 20(1), 50–67.
- Kamishima, T. (2003). Nantonac collaborative filtering: Recommendation based on order responses. In *Proceedings of the Ninth ACM SIGKDD International Conference on Knowledge Discovery and Data Mining, KDD '03*, New York, NY, USA, pp. 583–588. ACM.
- Kolde, R., S. Laur, P. Adler, and J. Vilo (2012). Robust rank aggregation for gene list integration and meta-analysis. *Bioinformatics* 28(4), 573–580.
- Lin, S. and J. Ding (2009). Integration of ranked lists via cross entropy Monte Carlo with applications to mRNA and microRNA studies. *Biometrics* 65(1), 9–18.
- Lu, T. and C. Boutilier (2011). Learning Mallows models with pairwise preferences. In L. Getoor and T. Scheffer (Eds.), *Proceedings of the 28th International Conference on Machine Learning, ICML '11*, New York, NY, USA, pp. 145–152. ACM.
- Luce, R. D. (1959). *Individual choice behavior: A theoretical analysis*. New York, NY, USA: Wiley.
- Luo, J., D. J. Duggan, Y. Chen, J. Sauvageot, C. M. Ewing, M. L. Bittner, J. M. Trent, and W. B. Isaacs (2001). Human prostate cancer and benign prostatic hyperplasia: Molecular dissection by gene expression profiling. *Cancer Research* 61(12), 4683–4688.
- Mallows, C. L. (1957). Non-null ranking models. I. *Biometrika* 44(1/2), 114–130.
- Marden, J. I. (1995). *Analyzing and Modeling Rank Data*, Volume 64 of *Monographs on Statistics and Applied Probability*. Cambridge, MA, USA: Chapman & Hall.
- Margolin, A. A., I. Nemenman, K. Basso, C. Wiggins, G. Stolovitzky, R. D. Favera, and A. Califano (2006). ARACNE: An algorithm for the reconstruction of gene regulatory networks in a mammalian cellular context. *BMC Bioinformatics* 7(Suppl 1), S7.

- Meilä, M. and H. Chen (2010). Dirichlet process mixtures of generalized Mallows models. In *Proceedings of the Twenty-Sixth Conference Annual Conference on Uncertainty in Artificial Intelligence (UAI-10)*, Corvallis, OR, USA, pp. 358–367. AUAI Press.
- Meyer, D. and K. Hornik (2009). Generalized and customizable sets in R. *Journal of Statistical Software* 31(2), 1–27.
- Meyer, D. and K. Hornik (2014). relations: Data structures and algorithms for relations. R package version 0.6-3.
- Mukherjee, S. (2013). Estimation of parameters in non uniform models on permutations. arXiv:1307.0978 [math.PR].
- Murphy, T. B. and D. Martin (2003). Mixtures of distance-based models for ranking data. *Computational Statistics & Data Analysis* 41(34), 645 – 655.
- Naume, B., X. Zhao, M. Synnestvedt, E. Borgen, H. G. Russnes, O. C. Lingjærde, M. Strømberg, G. Wiedswang, G. Kvalheim, R. Kåresen, J. M. Nesland, A.-L. Børresen-Dale, and T. Sørli (2007). Presence of bone marrow micrometastasis is associated with different recurrence risk within molecular subtypes of breast cancer. *Molecular Oncology* 1(2), 160 – 171.
- Plackett, R. L. (1975). The analysis of permutations. *Journal of the Royal Statistical Society. Series C (Applied Statistics)* 24(2), 193–202.
- Regenwetter, M., J.-C. Falmagne, and B. Grofman (1999). A stochastic model of preference change and its application to 1992 presidential election panel data. *Psychological Review* 106(2), 362–384.
- Singh, D., P. G. Febbo, K. Ross, D. G. Jackson, J. Manola, C. Ladd, P. Tamayo, A. A. Renshaw, A. V. D’Amico, J. P. Richie, E. S. Lander, M. Loda, P. W. Kantoff, T. R.

- Golub, and W. R. Sellers (2002). Gene expression correlates of clinical prostate cancer behavior. *Cancer Cell* 1(2), 203 – 209.
- Tan, A. C., D. Q. Naiman, L. Xu, R. L. Winslow, and D. Geman (2005). Simple decision rules for classifying human cancers from gene expression profiles. *Bioinformatics* 21(20), 3896–3904.
- True, L., I. Coleman, S. Hawley, C.-Y. Huang, D. Gifford, R. Coleman, T. M. Beer, E. Gelmann, M. Datta, E. Mostaghel, B. Knudsen, P. Lange, R. Vessella, D. Lin, L. Hood, and P. S. Nelson (2006). A molecular correlate to the gleason grading system for prostate adenocarcinoma. *Proceedings of the National Academy of Sciences* 103(29), 10991–10996.
- van Buuren, S. and K. Groothuis-Oudshoorn (2011). mice: Multivariate imputation by chained equations in R. *Journal of Statistical Software* 45(3), 1–67.
- Volkovs, M. N. and R. S. Zemel (2014). New learning methods for supervised and unsupervised preference aggregation. *Journal of Machine Learning Research* 15, 1135–1176.
- Welsh, J. B., L. M. Sapinoso, A. I. Su, S. G. Kern, J. Wang-Rodriguez, C. A. Moskaluk, H. F. Frierson, and G. M. Hampton (2001). Analysis of gene expression identifies candidate markers and pharmacological targets in prostate cancer. *Cancer Research* 61(16), 5974–5978.

Supplementary Material

This supplement is organized as follows. In Section S1, we describe the MCMC algorithm for the Mallows mixture model, and we state the posterior distributions for the time-dependent ranks. In Sections S2, S3, S4, S5, S6, S7, and S8, we give additional results for the potato experiment, meta analysis of gene lists, ranking of Premier League teams, sushi data, genomic data, Movielens data, and student data, respectively. Section S9 presents additional simulation results, and in Sections S10 and S11 we describe how the convergence of the Metropolis-Hastings algorithm and of the importance sampling algorithm were assessed.

S1 Technical Details

S1.1 MCMC Algorithm for Clustering

The MCMC algorithm alternates between sampling $\boldsymbol{\rho}_1, \dots, \boldsymbol{\rho}_G$ and $\alpha_1, \dots, \alpha_C$ in a Metropolis-Hastings step, and τ_1, \dots, τ_C and z_1, \dots, z_N in a Gibbs step. The former is straightforward, since $(\boldsymbol{\rho}_c, \alpha_c)_{c=1, \dots, C}$ are conditionally independent given z_1, \dots, z_N . In the latter, we exploit the fact that the Dirichlet prior for τ_1, \dots, τ_C is conjugate to the multinomial conditional prior for z_1, \dots, z_N given τ_1, \dots, τ_C . Thus,

$$\begin{aligned} P(\tau_1, \dots, \tau_C | \boldsymbol{\rho}_1, \dots, \boldsymbol{\rho}_G; \alpha_1, \dots, \alpha_C; z_1, \dots, z_N) &= P(\tau_1, \dots, \tau_C | z_1, \dots, z_N) \\ &\propto P(z_1, \dots, z_N | \tau_1, \dots, \tau_C) P(\tau_1, \dots, \tau_C) \propto \mathcal{D}(z_1, \dots, z_N; \psi + n_1, \dots, \psi + n_C), \end{aligned}$$

where $\mathcal{D}(\cdot)$ denotes the Dirichlet distribution and $n_c = \sum_{j=1}^N 1_c(z_j)$, $c = 1, \dots, C$. Therefore, in the Gibbs step for τ_1, \dots, τ_C , we sample from $\mathcal{D}(\psi + n_1, \dots, \psi + n_C)$. In the Metropolis-Hastings step, the proposal $\boldsymbol{\rho}'_c$ for each cluster is sampled from the leap-and-shift distribution,

and accepted with probability

$$\min \left\{ 1, \frac{\pi(\boldsymbol{\rho}'_c)}{\pi(\boldsymbol{\rho}_c)} \exp \left[\frac{-\alpha_c}{n} \sum_{j:z_j=c} \{d(\mathbf{R}_j, \boldsymbol{\rho}_c) - d(\mathbf{R}_j, \boldsymbol{\rho}'_c)\} \right] \right\}.$$

Next, if $C > 1$ and $c \notin \{1, C\}$, then $\alpha'_c \sim \mathcal{U}(\alpha_{c-1}, \alpha_{c+1})$; if $C > 1$ and $c = 1$ then $\alpha'_1 \sim \alpha_2 \mathcal{B}(5, 2)$; if $C > 1$ and $c = C$ then $\alpha'_C \sim \mathcal{U}(\alpha_{C-1}, \alpha_C + 1)$; and if $C = 1$, then $\alpha' \sim \mathcal{N}(\alpha, \sigma_\alpha^2)$.

This ensures that the components of $\boldsymbol{\alpha}'$ satisfy the ordering constraint $\alpha'_1 < \dots < \alpha'_C$. The proposed value α'_c is accepted with probability

$$\min \left\{ 1, \frac{Z_n(\alpha'_c)^{-n_c} \pi(\alpha'_c)}{Z_n(\alpha_c)^{-n_c} \pi(\alpha_c)} \exp \left[\frac{-(\alpha'_c - \alpha_c)}{n} \sum_{j:z_j=c} d(\mathbf{R}_j, \boldsymbol{\rho}_c) \right] \right\},$$

for $c = 1, \dots, C$. Finally, in the Gibbs step for z_j , $j = 1, \dots, N$, we sample from $P(z_j = c | \tau_c, \boldsymbol{\rho}_c, \alpha_c, R_j) \propto \tau_c P(\mathbf{R}_j | \boldsymbol{\rho}_c, \alpha_c) = \tau_c Z_n(\alpha_c)^{-1} \exp\{-(\alpha_c/n)d(\mathbf{R}_j, \boldsymbol{\rho}_c)\}$.

S1.2 Full Posteriors for Time-Dependent Ranks

The conditional distributions required in our MCMC algorithm for time-dependent ranks are

$$\begin{aligned} P\{\boldsymbol{\rho}^{(0:T)} | \text{data}, \alpha^{(0:T)}, \beta\} &\propto \\ &\left[\prod_{t=0}^T P\{\mathbf{R}_1^{(t)}, \dots, \mathbf{R}_{N_t}^{(t)} | \alpha^{(t)}, \boldsymbol{\rho}^{(t)}\} \right] \left[P\{\boldsymbol{\rho}^{(0)}\} \prod_{t=1}^T P\{\boldsymbol{\rho}^{(t)} | \boldsymbol{\rho}^{(t-1)}, \beta\} \right] \propto \\ &\exp \left[- \sum_{t=0}^T \frac{\alpha^{(t)}}{n} \sum_{j=1}^{N_t} d\{\mathbf{R}_j^{(t)}, \boldsymbol{\rho}^{(t)}\} - \frac{\beta}{n} \sum_{t=1}^T d\{\boldsymbol{\rho}^{(t)}, \boldsymbol{\rho}^{(t-1)}\} \right] \left[\prod_{t=0}^T 1_{\mathcal{P}_n}\{\boldsymbol{\rho}^{(t)}\} \right], \end{aligned}$$

$$\begin{aligned} P\{\alpha^{(0:T)} | \text{data}, \boldsymbol{\rho}^{(0:T)}, \sigma_\alpha\} &\propto \\ &\left[\prod_{t=0}^T P\{\mathbf{R}_1^{(t)}, \dots, \mathbf{R}_{N_t}^{(t)} | \alpha^{(t)}, \boldsymbol{\rho}^{(t)}\} \right] \left[P\{\alpha^{(0)}\} \prod_{t=1}^T P\{\alpha^{(t)} | \alpha^{(t-1)}, \sigma_\alpha^2\} \right] \propto \\ &\left[\prod_{t=0}^T Z_n\{\alpha^{(t)}\}^{-N_t} \right] \times \end{aligned}$$



Figure S1: Left: The 20 potatoes labeled by letters A-T. Right: Assessors in action.

$$\exp \left[- \sum_{t=0}^T \frac{\alpha^{(t)}}{n} \sum_{j=1}^{N_t} d \{ \mathbf{R}_j^{(t)}, \boldsymbol{\rho}^{(t)} \} - \sum_{t=1}^T \frac{\{ \alpha^{(t)} - \alpha^{(t-1)} \}^2}{2\sigma_\alpha^2} - \lambda \alpha^{(0)} \right],$$

$$P \{ \beta | \boldsymbol{\rho}^{(0:T)} \} \propto \left\{ \prod_{t=1}^T Z_n(\beta)^{-1} \right\} \exp \left[\frac{-\beta}{n} \sum_{t=1}^T d \{ \boldsymbol{\rho}^{(t)}, \boldsymbol{\rho}^{(t-1)} \} - \lambda \beta \right],$$

and

$$P \{ \sigma_\alpha^2 | \alpha^{(0:T)} \} \propto P(\sigma_\alpha^2) \prod_{t=1}^T P \{ \alpha^{(t)} | \alpha^{(t-1)}, \sigma_\alpha^2 \} \propto$$

$$(\sigma_\alpha^2)^{-(a+T/2)-1} \exp \left[- \frac{b + \frac{1}{2} \sum_{t=1}^T \{ \alpha^{(t)} - \alpha^{(t-1)} \}^2}{\sigma_\alpha^2} \right].$$

$P \{ \sigma_\alpha^2 | \alpha^{(0:T)} \}$ is an inverse gamma distribution with shape $a+T/2$ and scale $b + \frac{1}{2} \sum_{t=1}^T \{ \alpha^{(t)} - \alpha^{(t-1)} \}^2$, which means that we have a nice conjugacy property for σ_α^2 . In order to sample from the first three conditionals, we need to use the Metropolis-Hastings algorithm.

S2 Potato Experiment

S2.1 Data Collection

Figure S1 (left) shows the 20 potatoes laid out on a plate, marked by letters from A to T, and Figure S1 (right) shows some of the assessors performing the visual inspection part of the experiment. Table S1 shows the ranks given by the 12 assessors in the visual inspection experiment, and Table S2 shows the ranks given in the weighing experiment.

Assessor	A	B	C	D	E	F	G	H	I	J	K	L	M	N	O	P	Q	R	S	T
1	10	18	19	15	6	16	4	20	3	5	12	1	2	9	17	8	7	14	13	11
2	10	18	19	17	11	15	6	20	4	3	13	1	2	7	16	8	5	12	9	14
3	12	15	18	16	13	11	7	20	6	3	8	2	1	4	19	5	9	14	10	17
4	9	17	19	16	10	15	5	20	3	4	8	1	2	7	18	11	6	13	14	12
5	12	17	19	15	7	16	2	20	3	9	13	1	4	5	18	11	6	8	10	14
6	10	15	19	16	8	18	6	20	3	7	11	1	2	4	17	9	5	13	12	14
7	9	16	19	17	10	15	5	20	3	8	11	1	2	6	18	7	4	14	12	13
8	14	18	20	19	11	15	6	17	4	3	10	1	2	7	16	8	5	12	9	13
9	8	16	18	19	12	13	6	20	5	3	7	1	4	2	17	10	9	15	14	11
10	7	17	19	18	9	15	5	20	3	10	11	1	2	6	16	8	4	13	12	14
11	12	16	19	15	13	18	7	20	3	5	11	1	2	6	17	10	4	14	8	9
12	14	15	19	16	12	18	8	20	3	4	9	1	2	7	17	6	5	13	10	11
True rank	11	17	19	16	10	15	5	20	3	4	9	1	2	6	18	7	8	14	12	13
True weight	73	56	50	59	77	62	87	46	95	89	78	115	99	86	54	85	80	68	72	71

Table S1: Ranks given by the 12 assessors (rows) to the 20 potatoes (columns) in the visual inspection experiment. The true ranks, and the true weights in grams, are given in the two bottom rows.

Assessor	A	B	C	D	E	F	G	H	I	J	K	L	M	N	O	P	Q	R	S	T
1	10	17	19	15	6	16	4	20	2	5	11	1	3	7	18	8	9	14	12	13
2	13	18	19	16	10	15	5	20	4	3	12	1	2	6	17	8	7	11	9	14
3	11	16	20	15	10	14	6	19	9	4	7	1	3	2	18	5	8	17	12	13
4	10	17	19	16	11	15	5	20	3	4	9	1	2	6	18	8	7	12	14	13
5	11	17	19	16	6	15	4	20	2	8	12	1	3	5	18	10	7	13	9	14
6	9	16	18	15	10	17	8	19	3	7	11	2	1	4	20	5	6	14	12	13
7	9	17	19	16	11	15	5	20	3	8	10	1	2	7	18	6	4	14	12	13
8	12	17	19	18	9	15	5	20	3	4	10	1	2	8	16	7	6	14	11	13
9	9	16	19	18	12	14	6	20	5	2	8	1	4	3	17	10	7	15	13	11
10	10	17	19	16	7	15	4	20	3	9	11	1	2	5	18	8	6	13	12	14
11	11	16	18	15	12	17	7	20	3	4	10	1	2	6	19	8	5	14	9	13
12	12	16	19	15	10	17	8	20	3	4	9	1	2	6	18	5	7	14	11	13
True rank	11	17	19	16	10	15	5	20	3	4	9	1	2	6	18	7	8	14	12	13
True weight	73	56	50	59	77	62	87	46	95	89	78	115	99	86	54	85	80	68	72	71

Table S2: Ranks given by the 12 assessors (rows) to the 20 potatoes (columns) in the weighing experiment. The true ranks, and the true weights in grams, are given in the two bottom rows.

S2.2 Posterior Distributions for Ranks

Figure S2 shows the cumulative distribution functions for the total distance between the latent ranks and the true ranks, as measured by the footrule, Kendall and Spearman distances. The Mallows model with the footrule and Kendall distances turned out best in the weighing experiment, while the Mallows model with the Spearman distance performed best in the visual inspection experiment. Figures S3 and S4 show a selection of results from the two potato experiments. The true rank of the heaviest and lightest potatoes had strongly peaked distributions, while the distributions of the potatoes closer to middle in weight, had a larger spread, representing a greater uncertainty about their true rank. The improved precision of the weighing experiment over the visual one is also evident from comparing these two figures.

We now consider estimating the set of top-5 potatoes, neglecting their order, still using the full data. For each of the three models, the posterior probability of being among the

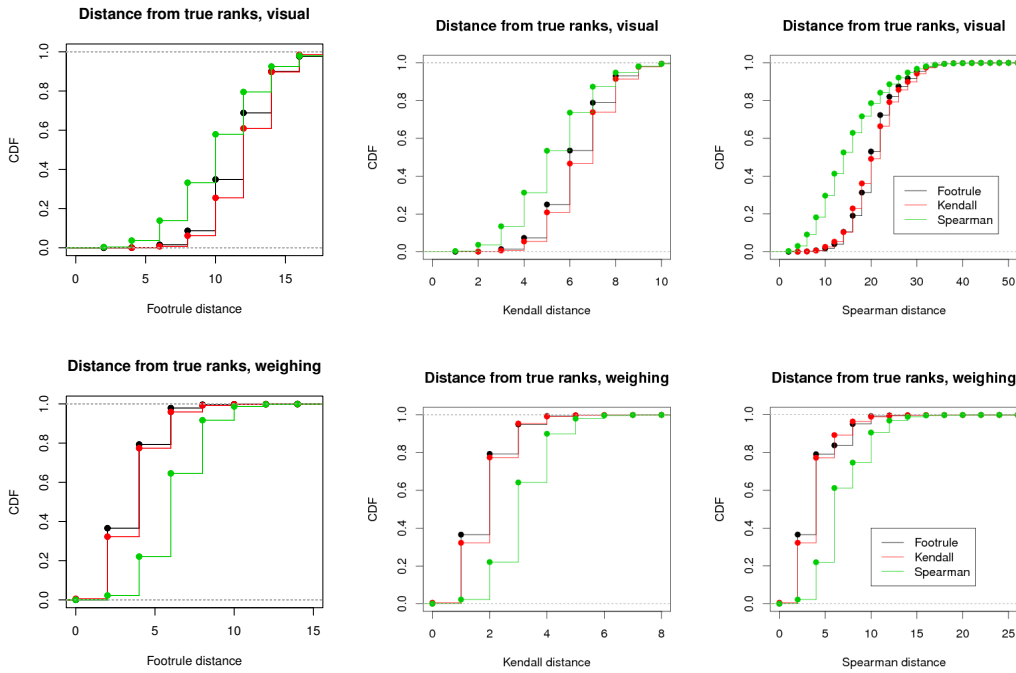


Figure S2: The posterior distributions, expressed in terms of the CDFs for the total distance between the latent and true ranks. The blue curves represent the posterior distributions for the latent ranks in the Mallows model with the footrule distance, the red curves with the Kendall distance, and the green curves with the Spearman distance.

Rank	Potato	Visual				Weighing			
		Footrule	Kendall	Spearman	Mean	Footrule	Kendall	Spearman	Mean
1	L	1.00	1.00	1.00	1.08	1.00	1.00	1.00	1.08
2	M	1.00	1.00	1.00	2.25	1.00	0.999	1.00	2.33
3	I	1.00	1.00	1.00	3.58	1.00	1.00	1.00	3.58
4	J	0.997	0.961	0.882	5.33	1.00	0.997	0.960	5.17
5	G	0.107	0.173	0.603	5.58	0.936	0.866	0.315	5.58
6	N	0.006	0.013	0.206	5.83	0.065	0.138	0.725*	5.42
7	P	0.000	0.000	0.000	8.42	0.000	0.000	0.000	7.33
8	Q	0.890*	0.852*	0.310	5.75				
9	K	0.000	0.000	0.000	10.33				
	⋮	⋮	⋮	⋮	⋮	⋮	⋮	⋮	⋮
	⋮	⋮	⋮	⋮	⋮	⋮	⋮	⋮	⋮
20	H	0.000	0.000	0.000	19.75	0.000	0.000	0.000	19.83

Table S3: The posterior probability of being among the top-5 for each potato. Numbers in boldface indicate credibility level of 95 % or higher, while asterisks indicate potatoes which were wrongly assessed to be top-5.

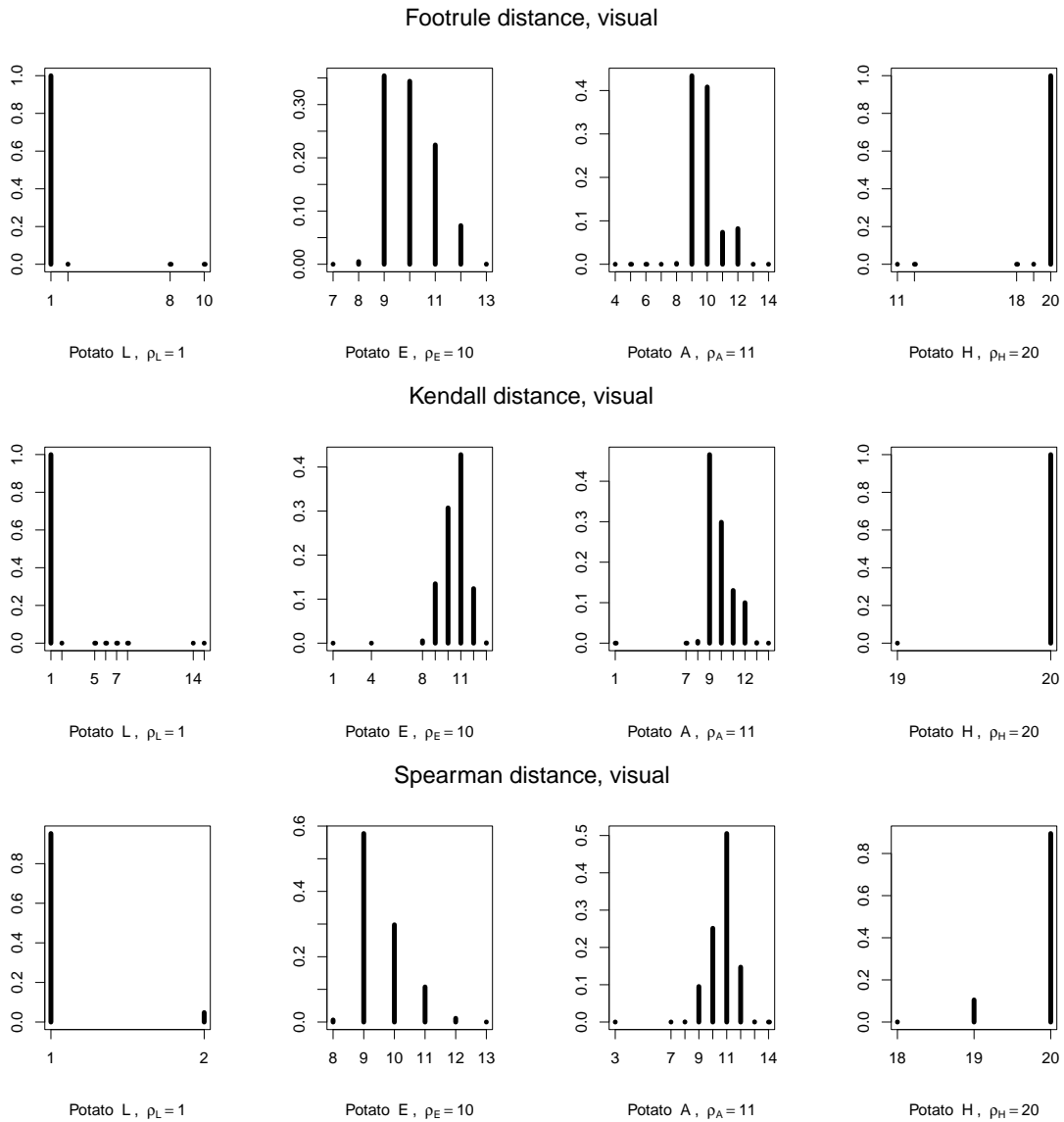


Figure S3: Posterior probabilities of the true ranks from the Mallows models in the visual inspection experiment, for the potatoes with true ranks 1 (heaviest), 10, 11 (middle), and 20 (lightest).

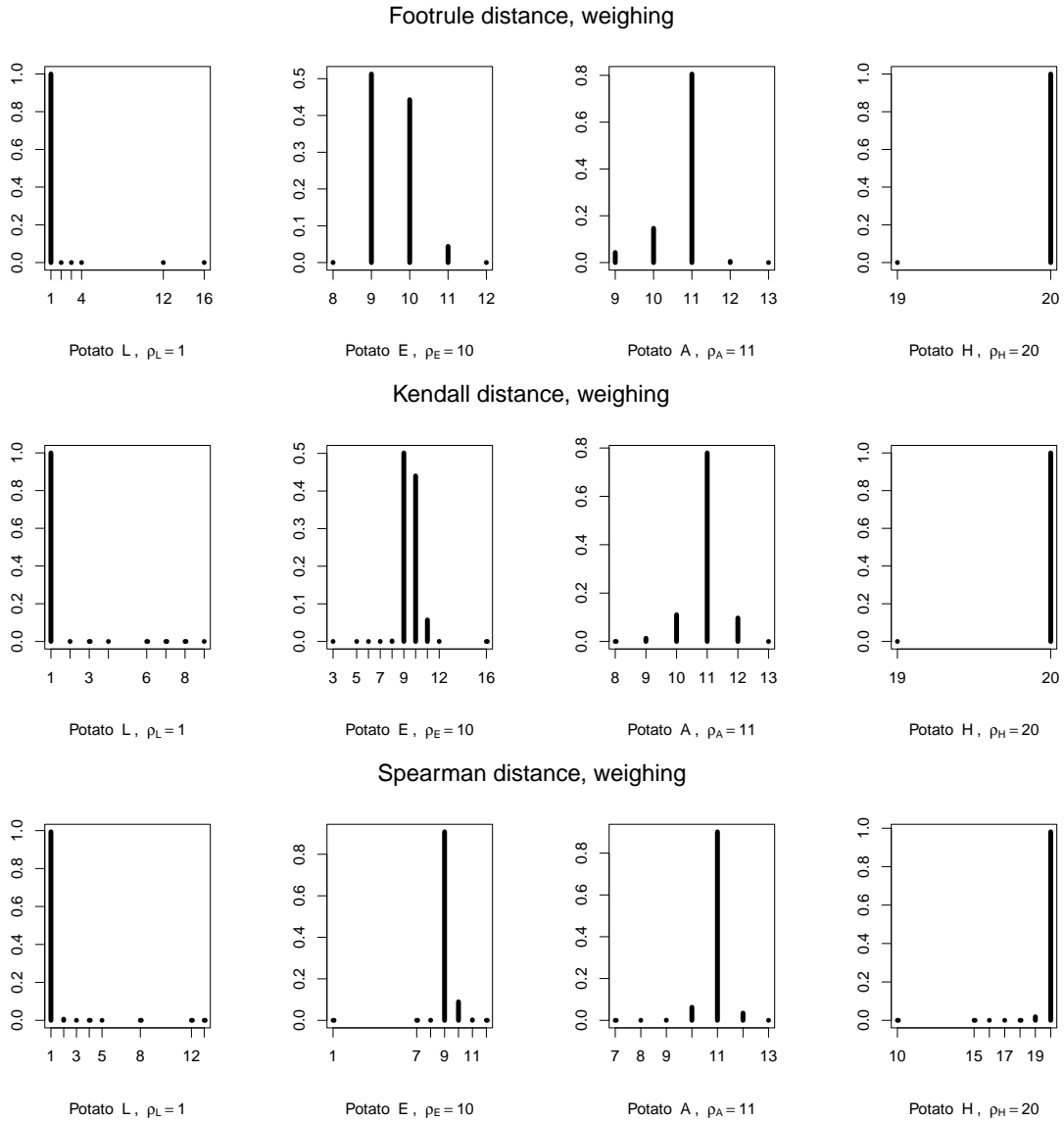


Figure S4: Posterior probabilities of the true ranks from the Mallows models in the weighing experiment, for the potatoes with true ranks 1 (heaviest), 10, 11 (middle), and 20 (lightest).

top-5 was computed for each potato, and is shown in the columns in Table S3. The potatoes are listed according to their true rank, and the mean ranking provided by the assessors is presented in the right column. The numbers in the columns for each model show, for each potato, the posterior probability that it is among the top-5. Defining the estimated top-5 set as the five potatoes with highest value of this posterior probability, we see from Table S3 that the Spearman model is the only one which identified the correct set of potatoes in the visual inspection experiment. (Both the footrule and the Kendall model gave potato Q, whose true rank was 8, a high probability of being among the top-5. The high posterior ranking given to potato Q can also be seen in the top left and center heat plots in Figure 1 of the main paper, as the red/yellow square which stands out below the diagonal at position 8 on the horizontal axis.) In the weighing experiment, both the footrule and Kendall model correctly identified the top-5, while the Spearman model included potato N (true rank 6) instead of potato G (true rank 5).

Table S3 and Figures S3 and S4 illustrate how the Bayesian framework easily allows for a quantification of the uncertainty in the estimates. In addition, we can compare the results obtained when using different distance measures, in contrast to most earlier work which have only used the Kendall distance. Here, the best results from the weighing experiment were obtained by applying the footrule distance, while use of the Spearman distance gave best results in the visual experiment.

S2.3 Partial Rankings

In Figure 2 of the main paper, we show the results of estimating the five heaviest potatoes based on either the top-5 or the top-10 rankings provided by each assessor in the weighing experiment. In Figure S5 we show the corresponding results for the visual inspection experiment. Again, the Mallows model with the footrule distance performed better than with the Kendall distance.

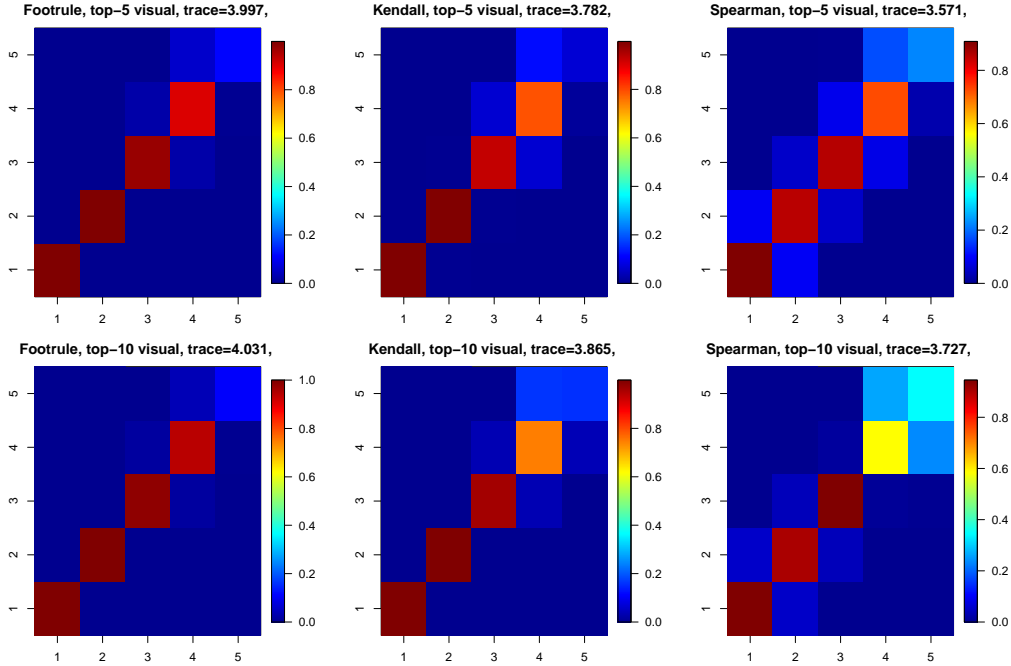


Figure S5: Estimation of the five heaviest potatoes when using only the five highest ranks from each assessor (top), and when using only the ten highest ranks from each assessor (bottom).

S2.4 Sensitivity to the Choice of Prior Distribution

In the potato experiment with full data, described in Section 4 of the main paper, we used an exponential prior for α with rate $\lambda = 1/10$ for the footrule and Kendall distances, and $\lambda = n/20$ for the Spearman distance. Here we investigate the sensitivity to the choice of this prior distribution for the Mallows model with the footrule distance in the visual experiment. Additional experiments of this type were also performed for the other Mallows models, as well as in the weighing experiment, and the results were similar. An exponential distribution with rate λ has mean $1/\lambda$, and variance $1/\lambda^2$, so a large value of λ implies a strong prior assumption that α is close to zero, and a correspondingly low precision in the measurements made by the assessors.

Figure S6 shows how the prior distribution for α influences the result. "Uniform" denotes a uniform improper prior distribution on the positive half line, $\pi(\alpha) = \mathcal{U}(0, \infty)$. We see that the uniform prior and the exponential prior with $\lambda = 1/10$ gave nearly identical posterior

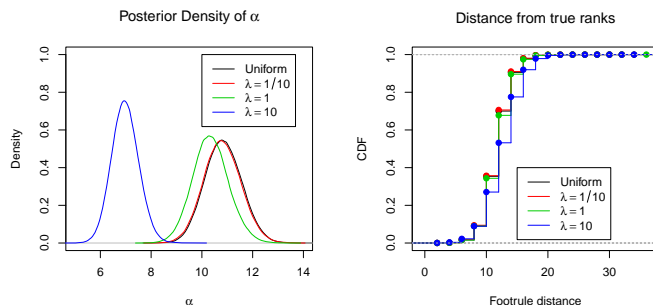


Figure S6: Impact of the prior distribution in the potato experiment with full data. Results are shown for the Mallows model with the footrule distance in the visual inspection experiment.

distributions for α , as well as posterior distributions for the distance from the estimated ranks to the true ranks. Setting $\lambda = 1$ resulted in a shift in the posterior distribution for α , but the distance to the true ranks was nearly unchanged. On the other hand, setting $\lambda = 10$ gave a strong shift to the left of the posterior distribution for α , and a clearly larger distance from the estimated ranks to the true ranks. We conclude that the model seems robust to small variations in the choice of λ in this case. Both $\lambda = 1$ and $\lambda = 10$ imply a very strong prior assumption that α is close to zero, and the model still produced reasonable results in these situations, with quite modest sample size.

In the top-5 experiment described in Section 5.1, we used less data than in the full data experiment. One could therefore suspect that the prior distribution is more important in this case. We thus repeated the experiment described above, and Figure S7 shows the resulting heat plots for the four different prior distributions for the Mallows model with the footrule distance, using the top-5 rankings of each assessors in the visual inspection experiment. Again we see that the results were essentially equal for the choices $\lambda = 1/10$ and $\lambda = 1$, as well as when the uniform prior was assumed. The extreme value $\lambda = 10$, on the other hand, yielded considerably worse performance.

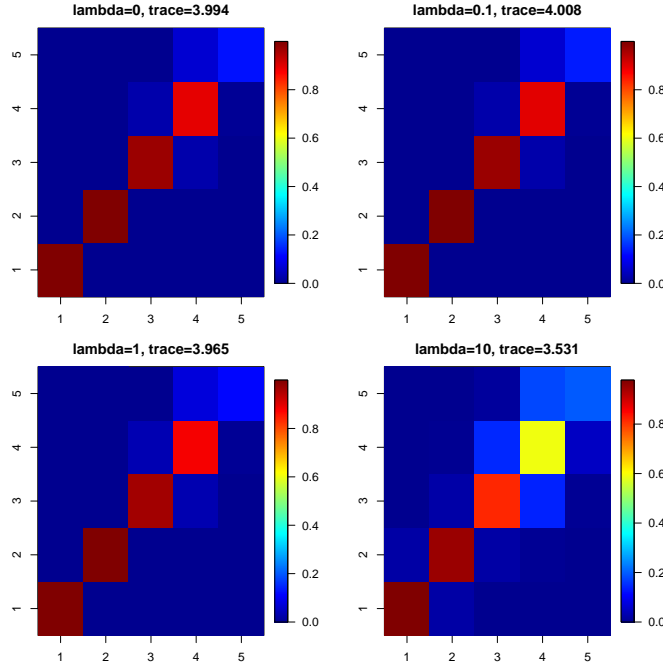


Figure S7: Impact of the prior distribution for α in the potato experiment, when the top-5 rankings of each assessor in the visual inspection part of the potato experiment were used, for the Mallows model with the footrule distance.

S3 Meta-Analysis of Differential Gene Expression

Table S4 shows the complete version of Table 1 in Section 5.2 in the main paper. Figure S8 shows the posterior distribution for α in the same experiment. Note that α is small, indicating a low level of agreement between the studies.

S4 Ranking of Premier League Teams

The Premier League data were downloaded from

http://clearlyandsimply.com/files/2010/05/premier_league.zip.

Figure S9 shows the posterior cumulative distribution functions for the ranks of the Premier League teams. The plots indicate that most teams are stochastically ordered: we say that team A_i dominates A_j , in the sense of stochastic ordering, if $P(\rho_i \leq r|\text{data}) \geq P(\rho_j \leq r|\text{data})$, $\forall r \in \{1, \dots, n\}$. We can also consider a stronger mode of ‘pointwise’

Rank	Gene	$P(\rho \leq \text{Rank})$	$P(\rho \leq 10)$	$P(\rho \leq 25)$
1	HPN	0.05	0.35	0.61
2	AMACR	0.06	0.27	0.53
3	GDF15	0.07	0.23	0.5
4	NME1	0.09	0.23	0.51
5	FASN	0.1	0.2	0.43
6	EEF2	0.12	0.19	0.43
7	UAP1	0.13	0.18	0.4
8	KRT18	0.14	0.17	0.39
9	OACT2	0.14	0.15	0.36
10	NME2	0.14	0.14	0.34
11	MTHFD2	0.15	0.14	0.35
12	CANX	0.17	0.14	0.34
13	SLC25A6	0.18	0.14	0.33
14	GRP58	0.19	0.14	0.34
15	SLC19A1	0.2	0.14	0.34
16	STRA13	0.2	0.13	0.31
17	PIB	0.22	0.13	0.32
18	MRPL3	0.23	0.13	0.31
19	ALCAM	0.24	0.12	0.31
20	TMEM4	0.24	0.11	0.31
21	MARCKS	0.25	0.12	0.3
22	CCT2	0.26	0.12	0.3
23	SND1	0.27	0.11	0.29
24	DAPK1	0.28	0.11	0.29
25	SAT	0.29	0.12	0.29

Table S4: Full version of Table 1 from the main paper.

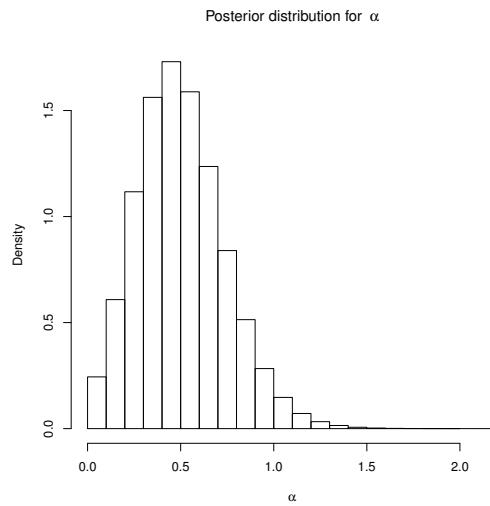


Figure S8: Posterior distribution for α in the meta analysis of gene lists.

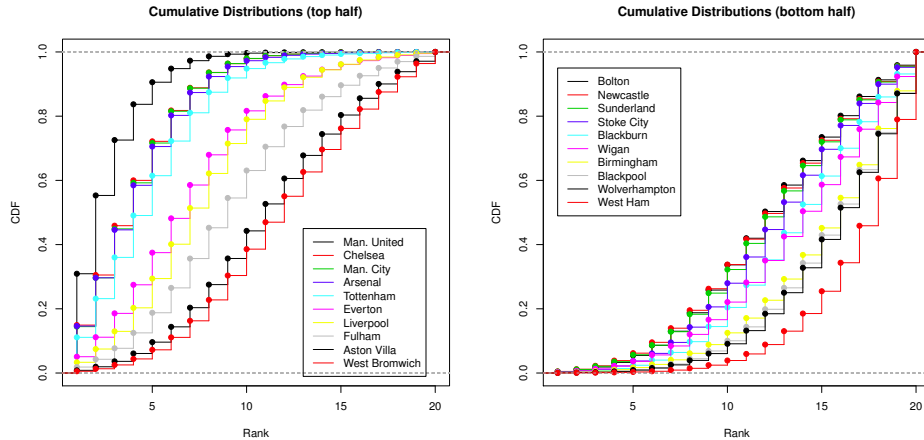


Figure S9: Posterior cumulative distribution functions for the ranks of the teams in the Premier League in the 2010/11 season.

ordering between teams and compute the posterior probability that team A_i has a lower rank than A_j , given by $P(\rho_i < \rho_j | \text{data})$. Table S5 summarizes these two measures for all the teams. The number in matrix entry (i, j) shows $P(\rho_i < \rho_j | \text{data})$, and if it is marked with an asterisk, team A_i stochastically dominates A_j . Out of the 190 pairs of teams, 182 were stochastically ordered. The remaining 8 pairs had matrix elements very close to 0.5. For example, the probability that Bolton has a higher rank than Newcastle was 0.51, and neither team dominated the other in the sense of stochastic ordering in our assessment.

S5 Clustering of the Sushi Data

The sushi dataset was downloaded from <http://kamishima.net/sushi/>. Figure S10 (left) shows the shift in the assignment of assessors to different clusters when a new cluster was added to the mixture. The figure is based on the MAP estimates of cluster assignments for $C \in \{1, \dots, 6\}$. The thickness of an arrow represents the proportion of assessors in the cluster who move along that route, and only flows bigger than 5% are displayed. The figure indicates some stability in the cluster memberships for different values of C .

We also analyzed the sushi data using the Spearman distance. Plotting the posterior

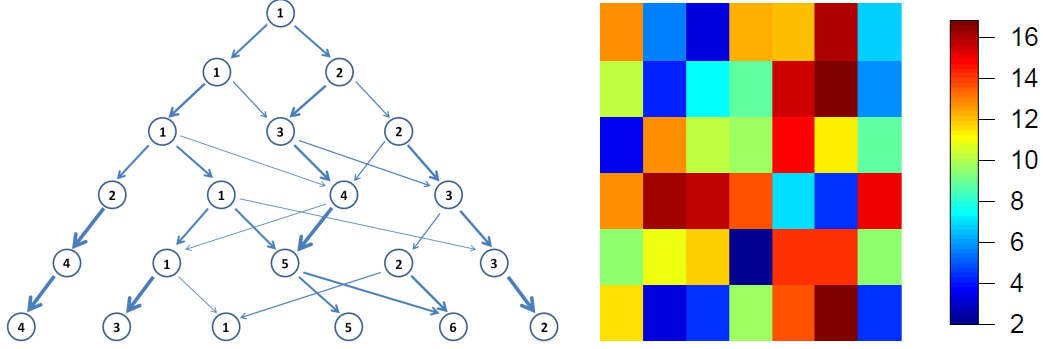


Figure S10: Left: Complementary plot for the Mallows mixture model with Spearman distance, described in Section 7.1 of the main paper. See Section S5 for description. Right: Pairwise Spearman distances between the MAP estimates of the cluster centers when using the footrule distance (along rows, $c = 1$ on top) or the Spearman distance (along columns, $c = 1$ to the left).

	$c = 1$	$c = 2$	$c = 3$	$c = 4$	$c = 5$	$c = 6$	$c = 7$
τ_c (%)	16.3(14.3,17.9)	12.5(11.1,14.7)	23.1(17.6,25.3)	10.4(9.24,12.0)	4.14(3.48,4.93)	4.67(3.91,5.63)	28.8(26.6,31.8)
α_c	0.72(0.67,0.76)	1.47(1.45,1.51)	1.82(1.80,1.86)	2.16(2.14,2.20)	2.41(2.39,2.45)	2.86(2.84,2.90)	3.49(3.47,3.53)
	fatty tuna tuna shrimp tuna roll squid sea eel egg cucumber roll salmon roe sea urchin	sea urchin fatty tuna salmon roe tuna shrimp squid tuna roll sea eel egg cucumber roll	fatty tuna sea eel sea urchin salmon roe tuna shrimp tuna roll squid egg cucumber roll	salmon roe fatty tuna tuna tuna roll shrimp egg squid sea eel cucumber roll sea urchin	shrimp salmon roe sea eel squid egg sea urchin cucumber roll tuna roll fatty tuna tuna	egg shrimp squid sea eel cucumber roll tuna tuna roll fatty tuna salmon roe sea urchin	fatty tuna tuna shrimp salmon roe sea urchin sea eel squid tuna roll egg cucumber roll

Table S6: Sushi items arranged according to the MAP estimates of the cluster centers (with Spearman distance), together with the corresponding MAP estimates for τ (in %) and α (with 95% HPD intervals).

distributions of the within-cluster sum-of-squares distances revealed an elbow at $C = 7$. Table S6 reports the MAP estimates for τ and α , together with their 95% HPDIs, and the sushi items arranged according to the MAP estimates of cluster centers, for each cluster. Figure S10 (right) reveals that five of the six clusters in Table 3 have a close neighbor among the ones in Table S6, i.e., $c = 1, 2, 3, 4, 5$ with the footrule correspond to $c = 3, 2, 1, 6, 4$ with the Spearman distance. Cluster 6 in Table 3 appears to combine elements from 2, 3, and 7 in Table S6, whereas cluster 5 in Table S6 has no close neighbor among the ones in Table 3.

S5.1 Convergence Checks

Some convergence plots are shown in Figures S11 and S12. In Figure S12 the trace plots of ρ_c for the first 4500 iterations of the MCMC algorithm are shown for all clusters and for

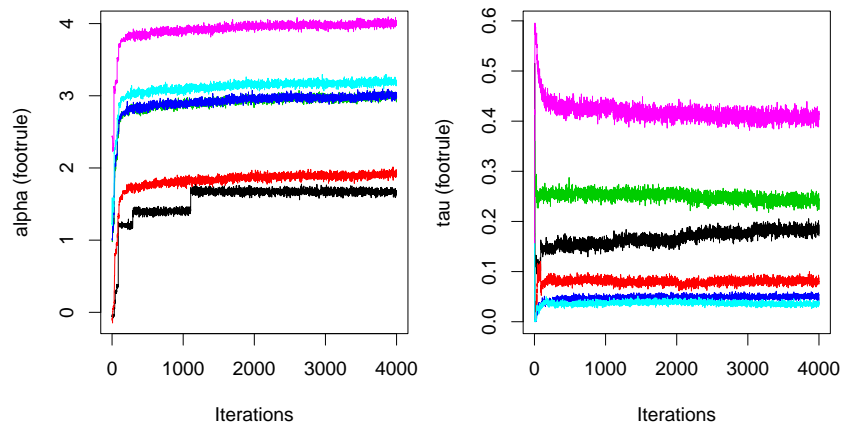


Figure S11: Cluster analysis of the sushi dataset when applying Mallows mixture models with the footrule distance and $C = 6$: trace plots of α_c (left) τ_c (right) and for the first 4000 iterations of the MCMC algorithm using a random starting point. Different colors refer to different clusters.

three sushi items: fatty tuna, which is always ranked high, cucumber roll, which is generally disliked, and shrimp, which is somehow in the middle. The trace plots corresponding to three random starting points are shown for each item. Different colors refer to different clusters. Similar plots for α_c and τ_c are shown in Figure S11.

S6 Classification of Genomic Data

The misclassification rates discussed in Section 8.1 of the main paper are based on the classification rule which assigns to ER+ or ER- according to the corresponding predictive probability of ER+ being above or below 0.5, respectively. It is worth exploring this choice further, in order to gain insight on the uncertainty associated to the classification. In Figure S13 (left), a histogram of the obtained posterior predictive probabilities of assignment to ER+ is shown. The green dots correspond to the posterior predictive probabilities of ER+ patients, the red dots to ER-. It can be seen that most of misclassified patients are the ones with the higher degree of uncertainty.

A good way of graphically illustrating the performance of a binary classifier as its dis-

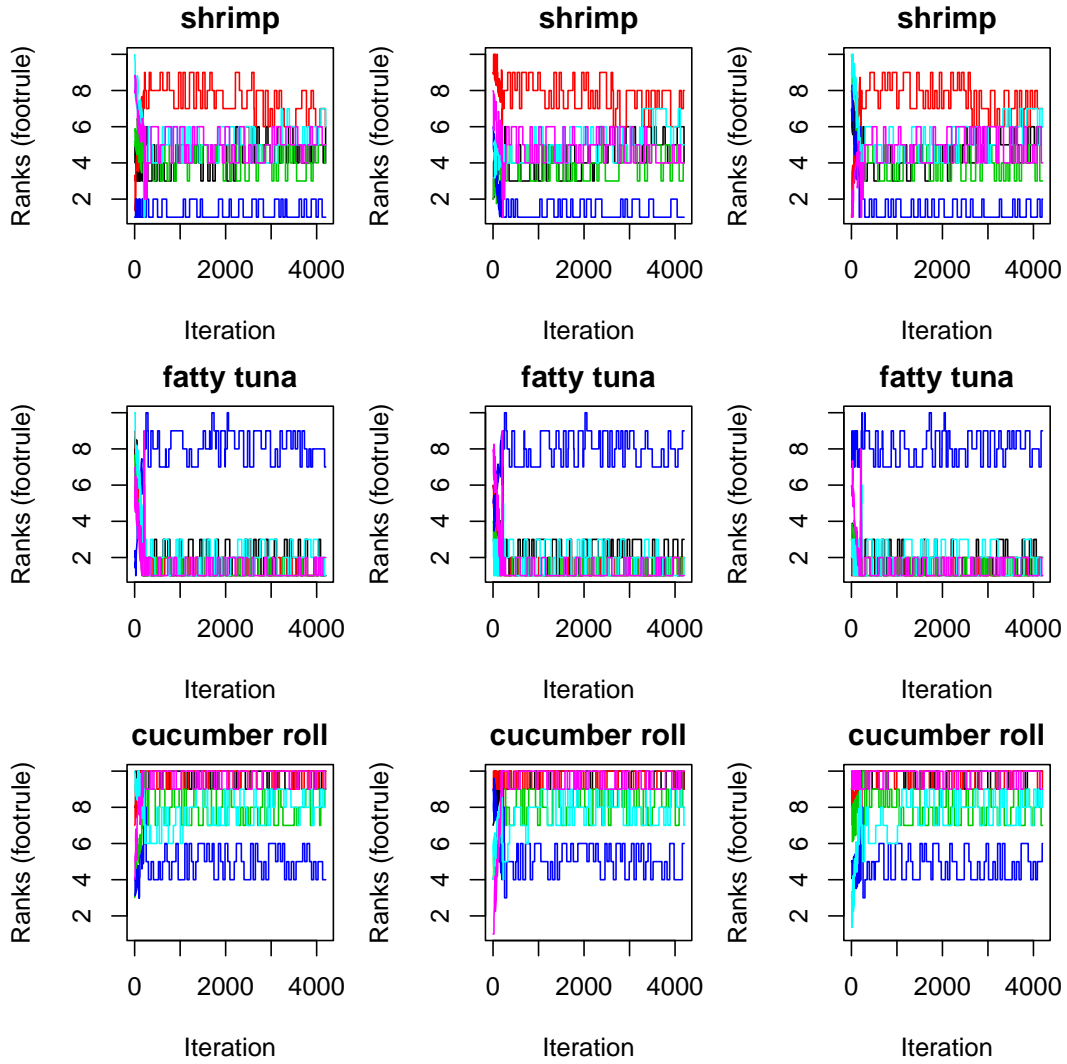


Figure S12: Cluster analysis of the sushi dataset when applying Mallows mixture models with the footrule distance and $C = 6$: trace plots of ρ_c for the first 4500 iterations of the MCMC algorithm for three sushi items (shrimp, fatty tuna, cucumber roll), using three random starting points. Different colors refer to different clusters.

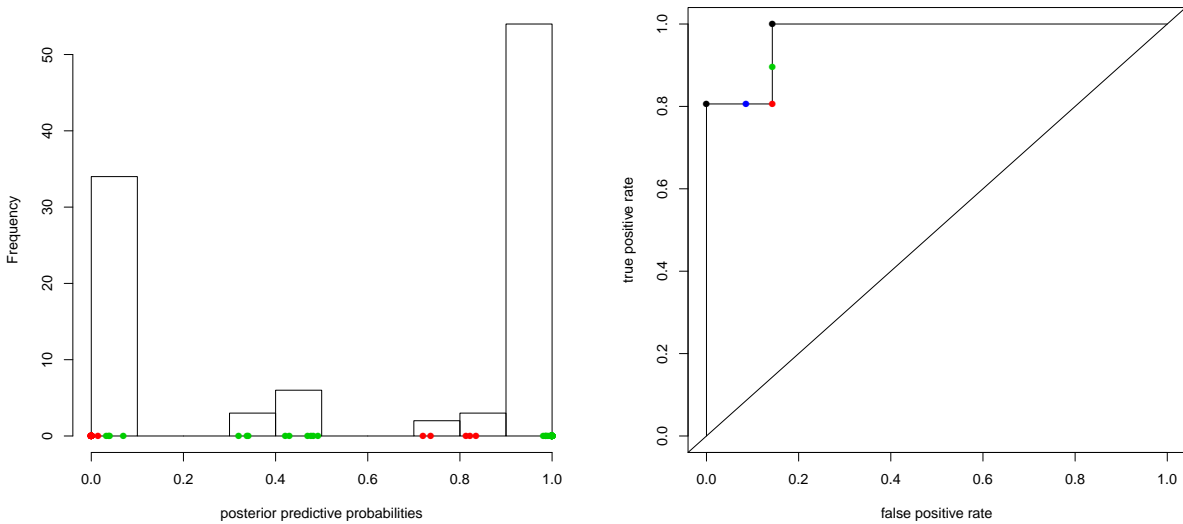


Figure S13: Left: histogram of posterior predictive probabilities of assignment to ER+ for patients in the genomic dataset. Red points refer to true ER- patients, green points to true ER+. Right: ROC curve for the assignment to ER+ or ER-; colored points refer to different thresholds on the posterior predictive for the assignment to ER+: green is 0.4, red is 0.5, blue is 0.8; the black dots refer to two extreme situations where false positives and false negatives can be avoided.

crimination threshold is varied is via a ROC curve. The curve is created by plotting the true positive rate (i.e., $P(\text{class} + | \text{ER}+)$) against the false positive rate (i.e., $P(\text{class} + | \text{ER}-)$) at various threshold settings. The threshold in this case is the cut-off for the posterior predictive, that for the results described in Section 8.1 had been set to 0.5. In Figure S13 (right) we show the ROC curve obtained by considering different thresholds for the predictive probabilities for classifying into ER+ and ER-. Some colored relevant points are also added, corresponding to some specific thresholds: green for 0.4, red for 0.5, blue for 0.8. The black dots correspond to extreme situations in which, by setting the threshold on the predictive probability of being assigned to ER+ to some values different from 0.5, one could achieve either 0 false positive rate (black point on the left) or 1 true positive rate (black point on the right). In other words, they can be summarized as “the best we can achieve with one class at the price of the other”, and they refer to thresholds of 0.835 and 0.033 if we privilege ER- and ER+, respectively.

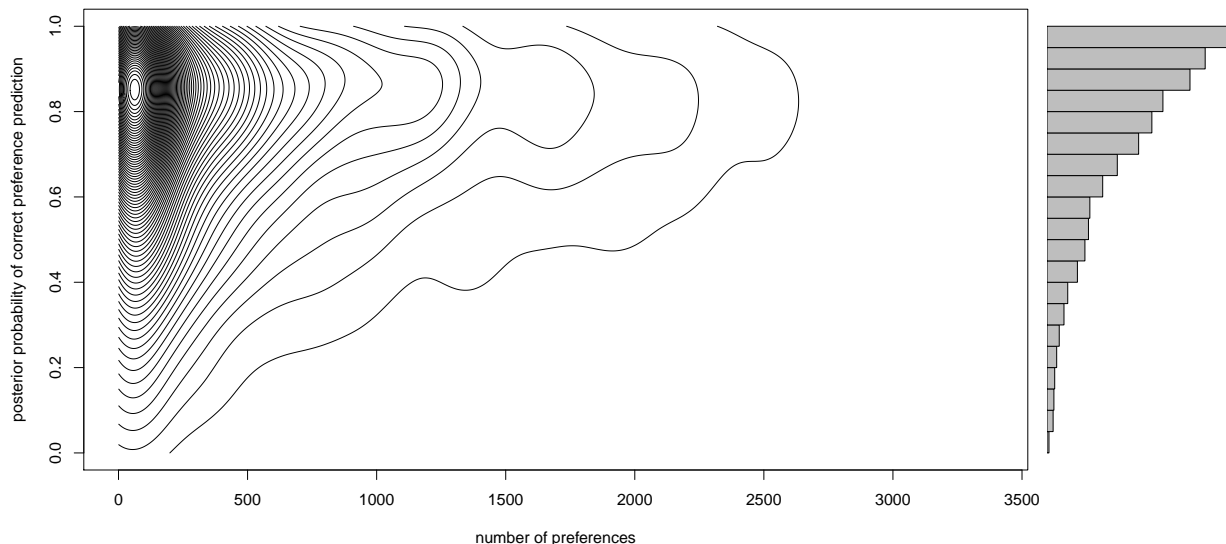


Figure S14: Movielens data: bivariate contour plot of the posterior probability of correctly predicting the discarded preference vs. the number of preferences stated by the assessor. The histogram on the right shows the marginal posterior probability of correct preference prediction.

S7 Preference Prediction for Movielens Data

The $N = 5891$ users included in the Movielens dataset were divided into 14 classes, based on gender and on the following age categories: “Under 18”, “18-24”, “25-34”, “35-44”, “45-49”, “50-55”, and “Over 55”.

Figure S14 shows a bivariate contour plot of the posterior probability of correct preference prediction vs. the number of preferences stated by the assessor. The histogram on the right shows the marginal posterior probability of correctly predicting the discarded preference for all assessors, regardless of how many preferences they had expressed.

A ROC curve as the one we displayed in Section S6 can be displayed also in the case of Movielens data, provided that we code the outcome in advance without looking at what the assessor actually thought. In other words, we systematically fix the event to be tested as $\{\text{assessed movie} \prec_j \text{deleted movie}\}$, and include in class 1 all assessors for whom this statement agrees with the preference actually expressed in the data. The resulting ROC curve is the one shown in Figure S15, corresponding to a AUC of 0.9417.

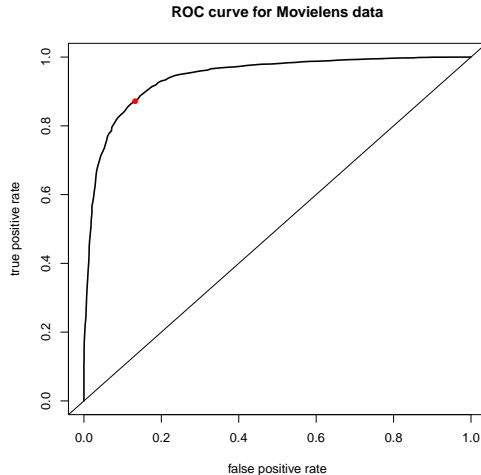


Figure S15: Movielens data: ROC curve. Classes are obtained by considering the event $\{\text{assessed movie} \prec_j \text{ deleted movie}\}$, and class 1 is formed by assessors whose preference agrees with the event. The red point corresponds to a threshold of 0.5 for the posterior predictive probability of assignment to the class 1.

S8 Student Data

The student data were collected by Prof. Roberta Micheli in the school years from 2002/2003 to 2005/2006, from her mathematics class at the technical high school “ITIS A. Volta” in Lodi, Italy. Table S7 shows the original data used in the analysis of time-dependent ranks in Section 9.1 of the main paper. Cells marked NA indicate missing values.

Figure S16 (left) shows the posterior density for $\alpha^{(t)}$ in each of the years. It is interesting to note that $\alpha^{(t)}$ increases with t . This indicates that the variation in the students’ performances was highest in the first year, and then gradually decreased. Figure S16 (right) shows the posterior density for β , from which it is clear that β is considerably larger than $\alpha^{(t)}$, $t = 0, 1, 2, 3$.

S9 Simulation Experiments

Figure S17 supplements Figure 5 in the main paper, by plotting the posterior mean footrule distance between the latent ranks and the true ranks, versus the number of leap-and-shift

	Year 1					Year 2					Year 3					Year 4									
	T1	T2	T3	T4	T5	T6	T7	T8	T9	T10	T11	T12	T13	T14	T15	T16	T17	T18	T19	T20	T21	T22	T23	T24	T25
1	5.5	5.3	5.3	9.5	9.0	9.0	8.0	6.3	NA	6.3	6.0	7.8	NA	5.5	7.3	7.3	6.3	NA	6.5	8.5	8.5	8.5	NA	7.75	
2	6.5	6.5	6.8	NA	8.0	6.5	8.0	6.0	7	5.8	5.3	6.5	6.5	NA	6.3	6.3	6	4.5	4.5	6.25	5.75	7	7.0	4	5.75
3	7.5	5.5	8.0	6.8	8.0	7.25	6.0	6.3	8	7	7.5	6.0	NA	5.3	8.5	8.5	7.3	8	6.75	6.75	6	5.75	5.5	6.5	6
4	5.5	NA	6.8	5.5	4.5	5.0	6.8	5.8	6.5	6	4.8	6.0	NA	4.3	4.0	4.0	5	7.25	NA	7.25	6	5.75	5.5	6.5	7.75
5	4.5	6.8	6.0	7.3	7.5	6.5	7.5	4.3	7	5.8	6.0	7.3	5.5	4.5	7.5	7.5	6.5	5.5	6.5	7.5	8.25	7.5	7.5	5	7.75
6	7.0	8.5	8.0	10	10.0	10.0	10.0	9.0	9.3	8.3	7.0	9.5	9	8.3	9.0	9.0	10	10	9	9.5	8.75	9.5	9.5	8.5	8.5
7	7.0	7.3	8.5	10	8.8	8.5	10.0	6.0	8.3	9.5	8.0	8.0	9.5	8.3	9.5	9.5	9.5	9.25	9.5	9.5	9	9.5	9.5	8.5	9
8	5.5	7	8.0	8.5	7.0	3.75	9.0	7.0	6.3	5.5	6.5	7.3	6	6	8.0	8.0	8.3	5.25	5.25	5.5	8	7.5	6.0	5.75	5.25
9	7.8	6.8	8.0	9.5	9.5	9.0	10.0	8.3	7.8	7.3	9.0	8.5	7.8	8.3	9.3	9.3	8.5	9.5	9.25	NA	7	8.75	8.25	8	7.75
10	4.0	6.5	7.8	7.3	8.0	6.0	7.3	6.0	8.5	5.3	6.0	7.8	7.3	3.5	5.0	5.0	6.5	6.5	5.25	6	NA	6.5	7.5	4	5.75
11	4.0	4.5	4.3	5	5.5	3.5	5.0	3.0	6.5	5	6.0	7.0	5	5.3	4.5	4.5	NA	6	NA	6	4.75	6	5.5	3	5
12	5.5	5	9.0	8.3	5.5	4.5	7.0	4.5	9.3	6.8	6.5	6.5	6	4.5	5.5	5.5	6	6	7	4.5	5	4	6.25	3	NA
13	6.8	7	7.3	6.5	9.0	7.5	9.5	8.0	9	NA	7.5	7.5	6.8	7.3	8.5	8.5	8.3	8.5	7	8	8.75	8.75	8.25	6	8.25
14	6.5	8	5.0	6	7.0	6.75	7.0	4.3	7	5.8	5.0	6.5	7.8	5	4.5	4.5	6.5	5	4	5.75	5	6.5	5.0	5.5	4.5
15	7.0	6.5	8.0	4.5	6.8	6.5	7.5	7.0	9	6	6.0	7.5	6	NA	8.0	8.0	NA	7.75	4.5	6	6	NA	5.0	8	6.75

Table S7: Test results for each of the 15 students over the 4 years. The individual tests are denoted T1, T2, up to T25.

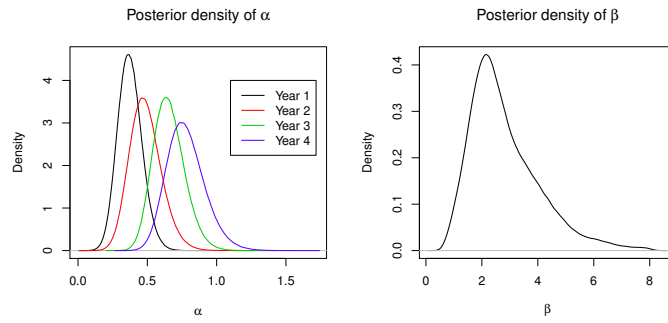


Figure S16: Posterior densities for $\alpha^{(t)}$ and β for the student data.

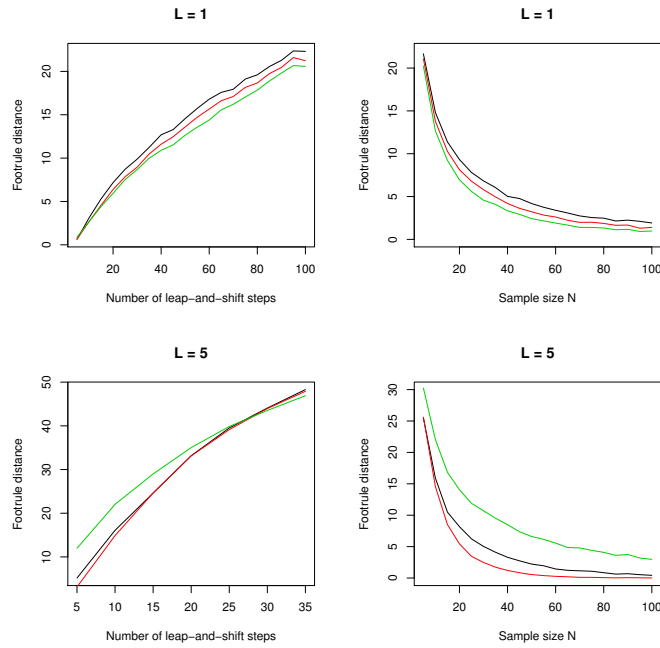


Figure S17: Mean footrule distance from the latent ranks to the true ranks as the number of leap-and-shift moves used to generate each observation increases (left), and as N increases (right), for the Mallows model with footrule distance (black curve), Kendall distance (red curve), and Spearman distance (green curve).

steps, and versus the sample size. The comparative performance of the Mallows models with the different distance measures shown here is in good agreement with Figure 5.

S9.1 Ranks Generated from a Mallows Model

In addition to the simulations described in Section 10 of the main paper, we conducted further experiments in which the ranks were generated from the three Mallows models with the footrule, Kendall, and Spearman distance. We set the number of assessors to $N = 10$, and the number of items to $n = 20$. For each value of α in a discrete range, we used the Metropolis-Hastings algorithm with fixed ranks $\boldsymbol{\rho} = (1, \dots, n)$ and fixed α to obtain N simulated samples. This was done by first running the algorithm until convergence, and then taking N observed ranks with a large enough interval between each sample to make them nearly independent. This gave a set $\mathbf{R}_1, \dots, \mathbf{R}_N$ of observed ranks, which was then used with the three distance measures, and the prior distributions described in Section 2.2 of the main paper. This gave three posterior distributions for latent ranks, one for each distance measure, and we finally found the mean posterior distance to the true ranks. We thus had a 3×3 design, with three models for generating samples and three for analyzing the observed ranks. The procedure was repeated 100 times for each value of α and each of the 9 settings. The values of α used for generating the observed ranks were 1, 2, 3, 4, 5, 6, 8, 10, 12, 14 with the footrule and Kendall distance, and the equivalent $1/n, 2/n, 3/n, 4/n, 5/n, 6/n, 8/n, 10/n, 12/n, 14/n$ with the Spearman distance.

Figure S18 shows the mean footrule distance from the posterior means to the true ranks over the 100 simulations. The error bars were very narrow, and hence omitted. Similar plots using the Kendall or Spearman distance on the vertical axis gave practically identical results, and are not shown. The left plot in Figure S18 shows the case in which the model with the footrule distance was used to generate the samples. In this case, it is clear that inference with the footrule distance that was used to generate the samples, gave the best results over the whole range of α values considered, although the difference between the models was rather

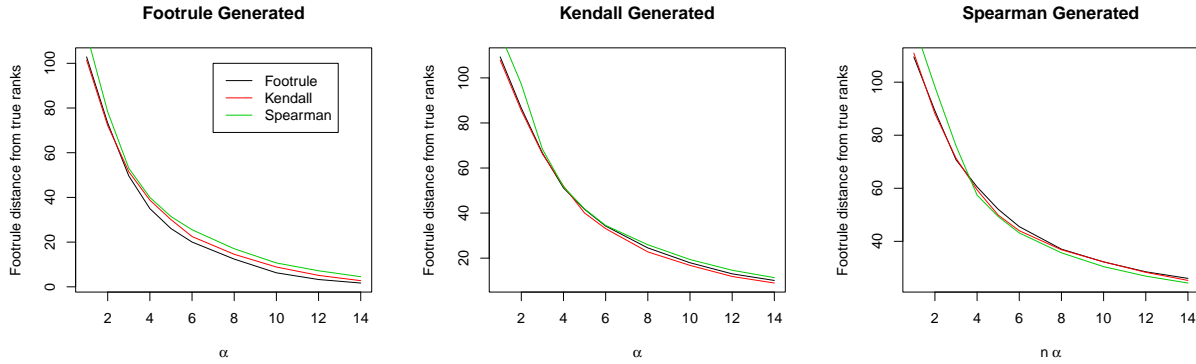


Figure S18: The plots from left to right show the mean distance between the posterior ranks and the true ranks in our simulation experiment, when the observed ranks were *generated* from the Mallows model with the footrule, Kendall, and Spearman distance, respectively. The black curves represent the ranks *estimated* with a Mallows model with the footrule distance, the red curves with the Kendall distance, and the green curves with the Spearman distance.

modest. The center plot shows the case in which the model with the Kendall distance was used to generate the samples. Here, it is harder to see any difference between the results obtained from the inference with the different distance measures. For small values of α , the Spearman distance gave poorer results, while the two other distances gave very similar results. For large values of α , on the other hand, the Kendall distance produced slightly better results than the other two. Finally, the right plot shows the results obtained for the samples generated with the Spearman distance. Here, it is interesting to see that inference with the footrule and Kendall distance was better than with the Spearman distance for small values of α , despite the fact that the samples were generated with the latter model. For α in the middle and upper range, on the other hand, inference with the Spearman distance gave slightly better results than the two other models. These experiments suggest that the Spearman distance is at a disadvantage when α is small, i.e., when the ranks are close to being uniformly distributed. For larger values of α , inference with the same model as was used to generate the data is slightly better than inference with any of the other two models.

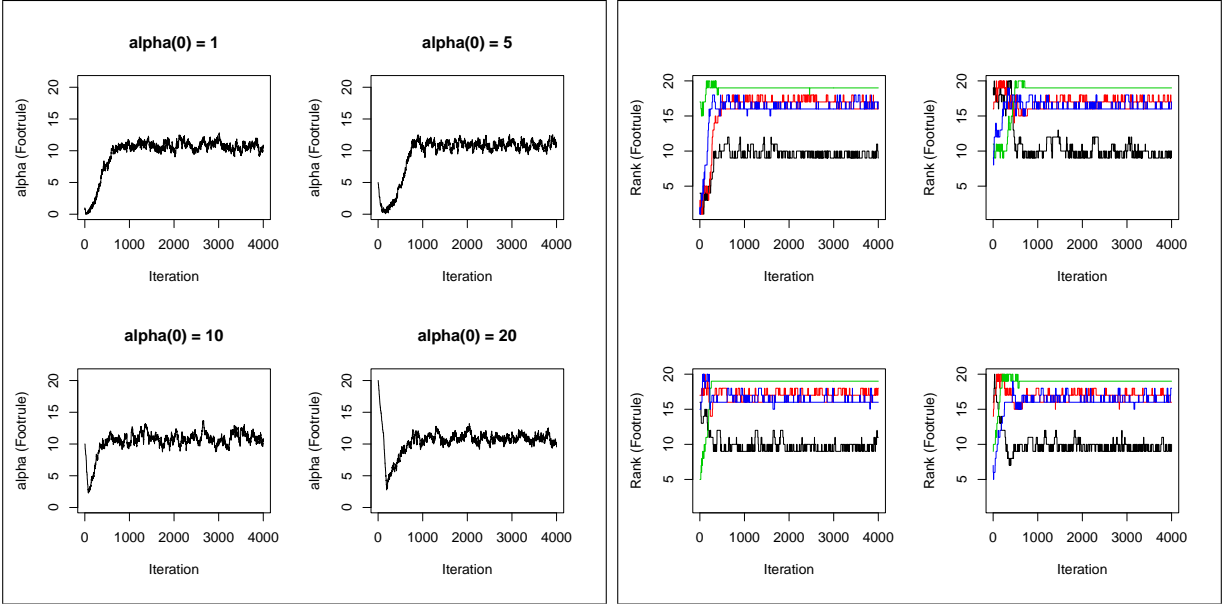


Figure S19: Convergence in the Mallows model with footrule distance. Left: Trace plots from four different initial values for α . Right: Trace plots for potatoes A (black line), B (red line), C (blue line), and D (green line) using four different random starting points for the rank vector.

S10 Convergence of Metropolis-Hastings Algorithm

Here we describe how to assess convergence of our Metropolis-Hastings algorithm, using examples from the potato experiment. Similar convergence assessments were performed for all the examples presented in the paper.

S10.1 Potato Experiment with Full Data

Figure S19 (left) shows trace plots of the first 4000 iterations of the MCMC algorithm using the footrule model and the data from the visual inspection experiment. The four plots show the traces for four different starting points. We see that after about 1000 iterations, α had converged to the same distribution in all cases. In each of the four runs, the starting points for the ranks were sampled uniformly from \mathcal{P}_n . Figure S19 (right) shows the corresponding trace plots for potatoes A, B, C, and D. Also here we see that the impact of the initial configuration was negligible after about 1000 iterations. The trace plots of the 16 remaining

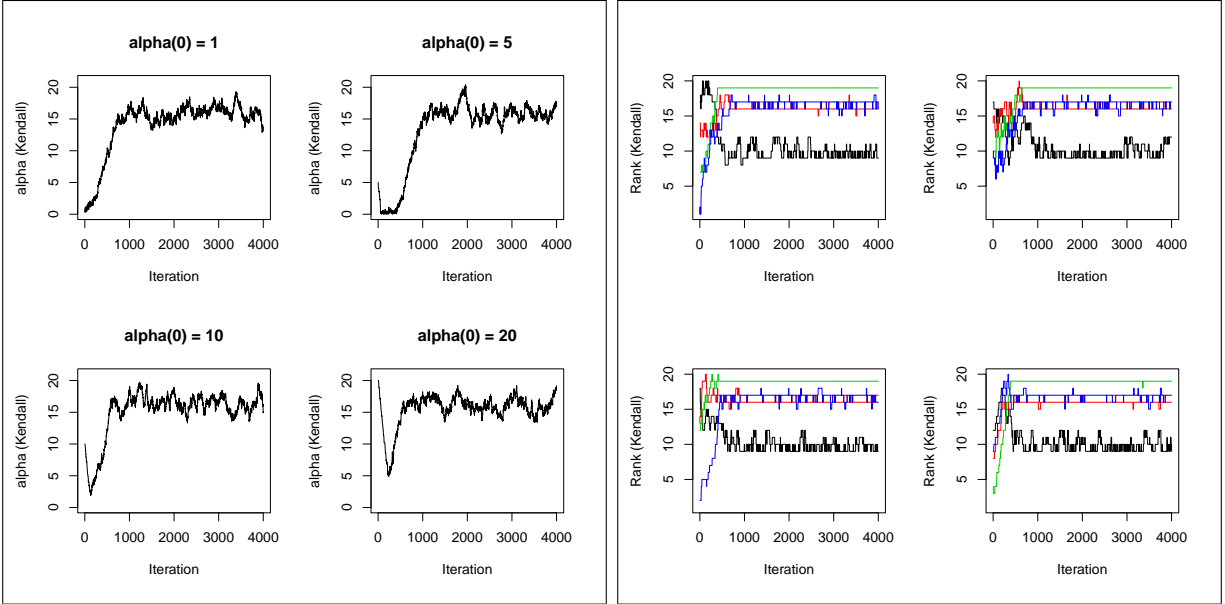


Figure S20: Trace plots for the Mallows Kendall model. See caption to Figure S19.

potatoes gave very similar results (not shown). Keeping in mind that Figure S19 shows traces of different parameters sampled from the same Markov chain, it is interesting to note that only one of the two plots is sufficient to assess convergence. When the algorithm starts, ρ has little agreement with the data, and therefore α is drawn towards zero, regardless of the starting point. Eventually, after some hundreds of iterations, ρ reaches configurations which agree more with the data, and α therefore increases again. We hence recommend trace plots of α as a simple tool for assessing convergence. In producing these plots, α' was sampled for $\mathcal{N}(\alpha, \sigma_\alpha^2)$, with $\sigma_\alpha = 0.04$, and ρ' from the leap-and-shift distribution with $L = 1$. Figure S20 shows the same plots for the Mallows model with the Kendall distance and Figure S21 for the Spearman distance. These plots also show good convergence after about 1000 iterations. For the Spearman model, we used $\sigma_\alpha = 0.0016$. Running each of the 4000 iterations took from 0.01 to 0.2 seconds on a desktop computer.

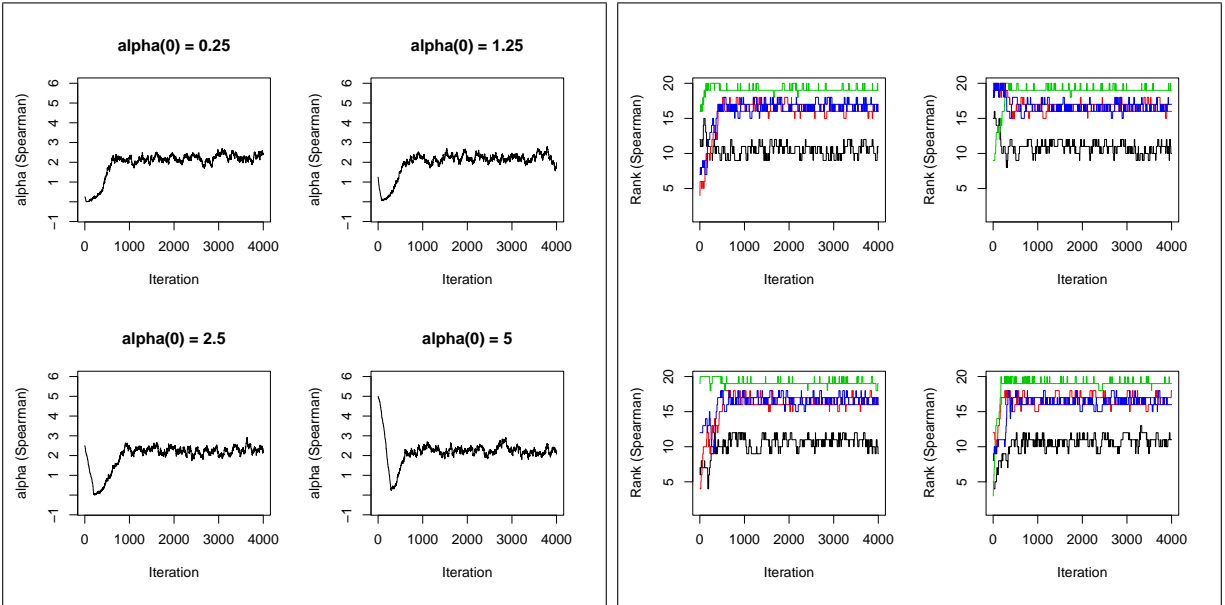


Figure S21: Trace plots for the Mallows Spearman model. See caption to Figure S19.

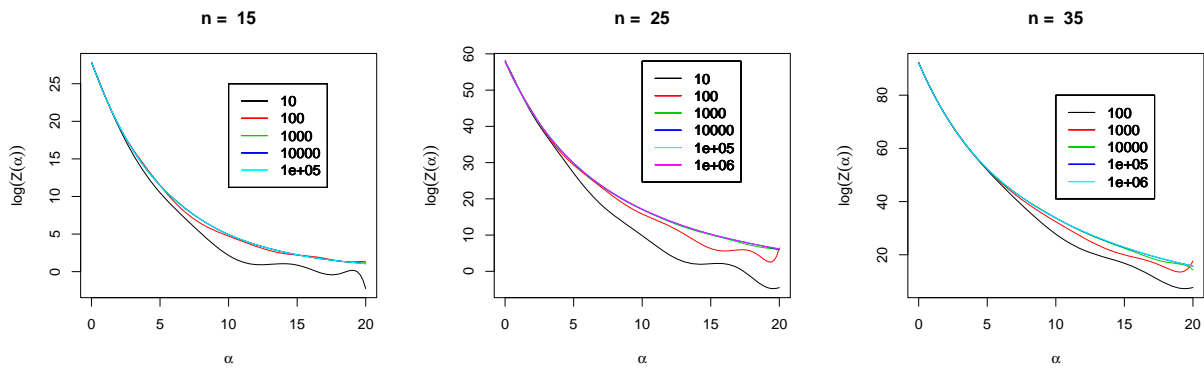


Figure S22: Estimates of the normalizing constant with the footrule distance using different numbers of Monte Carlo samples, specified by the legend.

S11 Convergence of Importance Sampler

This section illustrates the convergence of the importance sampler, and shows that it produces very good estimates of $\log\{Z_n(\alpha)\}$ using a number of samples many orders of magnitude smaller than the $n!$ terms in the exact expression. We present results for the case of the footrule distance, but similar results were obtained for the Spearman distance.

The importance sampler provides an estimate of $\log\{Z_n(\alpha)\}$, which we denote $\log\{\hat{Z}_n(\alpha)\}$. We first confirmed the consistency of the estimator by comparing the estimates to the exact sum for $n \leq 6$, seeing that the estimates perfectly overlapped the true function. For larger n , we determined the number of Monte Carlo samples necessary to obtain a sufficiently accurate estimate, by increasing the number of samples in powers of ten, and computing the difference between consecutive estimates. Between each two estimates, we measured the maximum relative change

$$\epsilon = \max_{\alpha} \left[\frac{\left| \log\{\hat{Z}_n(\alpha)\}_{new} - \log\{\hat{Z}_n(\alpha)\}_{old} \right|}{\left| \log\{\hat{Z}_n(\alpha)\}_{old} \right|} \right] \quad (\text{S1})$$

over a discrete grid of 100 equally spaced α values between 0.01 and 20.0. Finally, we estimated the normalizing constant with a polynomial of degree ten. For some of the examples shown in the paper, the grid of α values went up to 50.

Table S8 shows convergence results and Figure S22 shows the estimated functions. In the $n = 15$ case, the curves based on 10^3 and 10^4 are indistinguishable, although ϵ still is at 0.11 according to the table. Increasing to 10^5 Monte Carlo samples, ϵ is 0.01, and we are confident that the final estimate is very good. For comparison, computing the exact value of the normalizing constant would require summation of $15! \approx 10^{12}$ terms. For $n = 25$, ϵ between 10^5 and 10^4 samples was 0.03. In order to obtain ϵ of at most 0.01, we increased the final number of samples to 10^6 , which is much less than $25! \approx 10^{25}$. We conclude from this that the importance sampler yields very good estimates of the normalizing constant using a

number of samples which is much smaller than the number of terms in the exact sum. The computations shown here were performed on a desktop computer, and the computation with 10^6 samples for $n = 35$ took about an hour. Generating the Monte Carlo samples used in estimating the sum is perfectly parallelizable, so the computing time has the potential for significant reduction. If the number of samples is in the hundreds, it may be necessary to use parallel computation on a cluster in order to obtain a good estimate in reasonable time.

MC samples	Max. relative change, ϵ		
	$n = 15$	$n = 25$	$n = 35$
10			
10^2	277.48	165.24	
10^3	0.14	1.48	1.29
10^4	0.11	0.07	0.23
10^5	0.01	0.03	0.09
10^6		0.00	0.00

Table S8: The table shows how the convergence of the importance sampler for the footrule model depends on the number of samples used in the importance sampler. Each row shows the maximum relative incremental error between the current and the previous number of Monte Carlo samples, as specified by (S1).